



BAd-CRISPR: Inducible gene knockout in interscapular brown adipose tissue of adult mice

Received for publication, June 24, 2021, and in revised form, October 26, 2021 Published, Papers in Press, November 11, 2021,
<https://doi.org/10.1016/j.jbc.2021.101402>

Steven M. Romanelli¹, Kenneth T. Lewis¹, Akira Nishii¹, Alan C. Rupp², Ziru Li¹, Hiroyuki Mori¹, Rebecca L. Schill¹, Brian S. Learman¹, Christopher J. Rhodes³, and Ormond A. MacDougald^{1,2,*}

From the ¹Department of Molecular & Integrative Physiology, and ²Department of Internal Medicine, University of Michigan Medical School, Ann Arbor, Michigan, USA; ³Research and Early Development, Cardiovascular, Renal and Metabolism (CVRM), BioPharmaceuticals R&D, AstraZeneca, Gaithersburg, Maryland, USA

Edited by Qi-Qun Tang

CRISPR/Cas9 has enabled inducible gene knockout in numerous tissues; however, its use has not been reported in brown adipose tissue (BAT). Here, we developed the brown adipocyte CRISPR (BAd-CRISPR) methodology to rapidly interrogate the function of one or multiple genes. With BAd-CRISPR, an adeno-associated virus (AAV8) expressing a single guide RNA (sgRNA) is administered directly to BAT of mice expressing Cas9 in brown adipocytes. We show that the local administration of AAV8-sgRNA to interscapular BAT of adult mice robustly transduced brown adipocytes and ablated expression of adiponectin, adipose triglyceride lipase, fatty acid synthase, perilipin 1, or stearoyl-CoA desaturase 1 by >90%. Administration of multiple AAV8 sgRNAs led to simultaneous knockout of up to three genes. BAd-CRISPR induced frame-shift mutations and suppressed target gene mRNA expression but did not lead to substantial accumulation of off-target mutations in BAT. We used BAd-CRISPR to create an inducible uncoupling protein 1 (*Ucp1*) knockout mouse to assess the effects of UCP1 loss on adaptive thermogenesis in adult mice. Inducible *Ucp1* knockout did not alter core body temperature; however, BAd-CRISPR *Ucp1* mice had elevated circulating concentrations of fibroblast growth factor 21 and changes in BAT gene expression consistent with heat production through increased peroxisomal lipid oxidation. Other molecular adaptations predict additional cellular inefficiencies with an increase in both protein synthesis and turnover, and mitochondria with reduced reliance on mitochondrial-encoded gene expression and increased expression of nuclear-encoded mitochondrial genes. These data suggest that BAd-CRISPR is an efficient tool to speed discoveries in adipose tissue biology.

Adipose tissues play important physiological roles in the maintenance of whole-body energy homeostasis and metabolism. Beyond simply storing excess energy in the form of triacylglycerols, adipose tissues are found throughout the body in distinct depots, each with unique functions. Classically, adipose tissues are categorized as white (WAT), which are

found in subcutaneous and visceral depots, or brown (BAT), which are found in the interscapular, periaortic, perirenal, paravertebral, and intercostal depots (1, 2). Beige/BRITE adipocytes, a distinct adipocyte population induced by cold exposure and adrenergic agonists, are found within a subset of WAT depots (3). Adipose tissues are also located in more specialized areas, such as in the bone marrow, intramuscular, periarticular, pericardial, epicardial, retro-orbital, and dermal depots (1, 4, 5). Collectively, these tissues comprise the largest endocrine organ in the body and regulate satiety, carbohydrate and lipid metabolism, bone homeostasis, blood pressure, and the immune response (6, 7). Thus, investigation of adipose tissues is integral to our understanding of their roles in metabolic disorders such as obesity or lipodystrophy (8).

Research on adipose tissues has relied heavily on transgenic mouse models. Conditional models using the Cre/LoxP system have enabled tissue-specific knockouts to study genes of interest. Several Cre-recombinase lines have been developed in which adipose-Cre expression is driven by promoters/enhancers for adiponectin (*Adipoq*), *Fabp4*, *PdgfRa*, *Prx1*, or uncoupling protein 1 (*Ucp1*) (9–11). In addition, inducible transgenic models including *Adipoq-Cre*^{ERT}, *Ucp1-Cre*^{ERT}, and “AdipoChaser” have afforded control over the timing of gene knockout (9, 10, 12, 13). Although these transgenic mouse models have led to tremendous advances in our understanding of adipose tissue development and physiology, they are not without limitations. For example, *Adipoq-Cre* causes recombination in some osteoblasts, whereas *Fabp4-Cre* causes widespread recombination due to early expression in development (9, 11, 14, 15). Moreover, tamoxifen administration to *Cre*^{ERT} mice has been shown to decrease food intake and adipose mass, and in some cases, interact with the genetic deficiency to influence the resulting phenotype (16). Cre expression can also change from generation-to-generation in mouse colonies (14). Another critical limitation is that Cre mice must be bred to mice harboring a floxed allele, which necessitates the generation of a new mouse strain. Generating novel transgenic strains requires a substantial investment of time and financial resources before experiments can be performed, and knocking out multiple genes is possible but onerous. Therefore, the field would benefit from more

* For correspondence: Ormond A. MacDougald, macdouga@umich.edu.

BAd-CRISPR: Inducible gene knockout in BAT of adult mice

efficient strategies to investigate gene function in adipose tissues.

An alternative strategy to modulate gene expression *in vivo* has centered upon the use of CRISPR/Cas9 delivery for inducible knockout in somatic tissues. CRISPR/Cas9 comprises a Cas9 endonuclease, which creates double-strand DNA breaks, and a single guide RNA (sgRNA), which is a programmable RNA molecule that directs Cas9 to its target site for mutagenesis (17, 18). Both the Cas9 endonuclease and sgRNA can therefore be genetically encoded and packaged into a virus for somatic knockout in adult tissues (19). Viral delivery of the CRISPR/Cas9 machinery for inducible gene deletion offers several advantages over conventional germline knockouts as the timing, tissue, and target can be closely controlled (19). Moreover, embryonically lethal genes can be studied in this context. Several iterations of viral CRISPR/Cas9 delivery have been developed (20). For example, both Cas9 and sgRNA have been packaged into viral vectors and administered to the lung epithelium, liver, and hippocampus (21–23). In addition, transgenic approaches have created inducible and tissue-specific Cas9-expressing mouse models to which sgRNAs are delivered using adeno-associated viruses (AAVs) (20). Platt *et al.* (24) developed a Cre-dependent Cas9 knockin mouse, which when bred to mice expressing Cre enables somatic genome editing in specific tissues. As a proof of concept, AAVs encoding a sgRNA to *Kras*, *p53*, or *Lkb1* were delivered to the lung to accurately model adenocarcinoma disease progression. This Cas9 model has been further adapted for inducible somatic gene knockout in heart, skin, intestine, and thymus, thereby demonstrating its broad versatility across different tissues (25, 26).

Although AAV-mediated CRISPR/Cas9 gene transfer has proven useful for modeling disease in numerous tissues, its use in adipose tissues has been limited. This, in part, is because adipose tissues are located throughout the body, making transduction difficult (27–29). Moreover, mature adipocytes only comprise 11 to 40% of the total cell population of adipose tissues and lack unique cell-surface receptors, which make it challenging for vectors to navigate specifically to the adipocytes (27–29). Currently, mutagenesis by CRISPR/Cas9 has been accomplished in preadipocyte culture models and in posterior subcutaneous WAT (psWAT). For example, Shen *et al.* (30) transduced primary preadipocytes using a nonviral vector to administer CRISPR/Cas9 and disrupt expression of the *Nrip1* gene. In another study, Kamble *et al.* (31) electroporated CRISPR/Cas9 into human preadipocytes and demonstrated efficient knockout of *Pparg* and *Fkbp5*. Although these studies show that CRISPR/Cas9 can function in cultured preadipocyte models, the field has yet to unlock the full potential of CRISPR/Cas9 for somatic gene editing *in vivo*. Toward that goal, the Rosen laboratory used AAV-mediated CRISPR/Cas9 mutagenesis to inducibly knockout *Herc6* in inguinal WAT and suppress the expression of *Herc6* mRNA in adipocytes (32). Although this study demonstrated that CRISPR/Cas9 can be used in adipose tissue, it did not fully characterize its application or evaluate utility in BAT. Thus, we optimized AAV-mediated CRISPR/Cas9 to knockout genes in

interscapular BAT, which is an important site of adaptive thermogenesis and uncoupled oxidative phosphorylation (33). BAT also secretes endocrine and local factors that stimulate thermogenesis by increasing hypertrophy, vascularization, innervation, and blood flow to BAT (34). In humans, active BAT is inversely associated with body mass index, making it a potentially attractive target for combatting obesity (35).

Herein, we report the use of CRISPR/Cas9 to induce gene knockout in BAT. Our methodology, termed brown adipocyte CRISPR (BAd-CRISPR), integrates viral delivery with the established Cre/LoxP approach to significantly decrease the time and investment required to knockout genes in the BAT of adult mice. We accomplished this by administering AAV8-sgRNA to brown adipocyte-specific Cas9 expressing mice. BAd-CRISPR efficiently targeted *Adipoq*, adipose triglyceride lipase (*Atgl*), fatty acid synthase (*Fasn*), perilipin 1 (*Plin1*), stearoyl Co-A desaturase 1 (*Scd1*), or *Ucp1* in BAT, decreasing expression by 80 to 99%. We also showed that BAd-CRISPR inducible gene knockout recapitulates previously reported phenotypes for *Atgl*, *Plin1*, and *Fasn* knockout mice. Importantly, we show that BAd-CRISPR streamlines the path to generate transgenic mice, and affords the ability to disrupt the expression of up to three genes simultaneously in interscapular BAT. Lastly, we used BAd-CRISPR to create inducible *Ucp1* knockout mice and found that loss of UCP1 in adult mice did not impair adaptive thermogenesis following cold exposure. However, we observed an increase in circulating fibroblast growth factor 21 (FGF21), alterations to mitochondrial gene expression, and dramatic changes to the transcriptome predicted to increase heat production through peroxisomal lipid oxidation and futile cycling through elevated protein synthesis and degradation. Thus, BAd-CRISPR is an effective approach for generation of inducible knockouts to study gene function in interscapular BAT of adult mice.

Results

Transfection of adipocyte precursors with sgRNAs predominantly causes frameshift mutations in the target gene

To induce gene knockout in adult mice, we devised the BAd-CRISPR method, in which AAV-sgRNAs are administered to mice expressing Cas9 in brown adipocytes. We created a cloning strategy that facilitates incorporation of a U6 promoter-driven sgRNA into an AAV expression vector (Fig. S1A). The AAV expression vector also contains a CMV-driven mCherry fluorescent marker and 5' and 3' inverted terminal repeats (Fig. 1A). We designed sgRNAs using the CRISPOR design tool and selected sgRNAs that targeted early coding regions, lacked 0- or 1-base mismatch off-target sites, and had high cutting frequency determination (CFD) scores (36). The CFD score, developed by Doench and Fusi, calculates the off-target potential of a sgRNA by considering the positions and identities of mismatched nucleotides in the sgRNA sequence (37). As a general rule, sgRNAs should have a CFD score ≥ 0.2 (37). All of the sgRNAs used in the following studies had a CFD score > 0.4 (Fig. S1B).

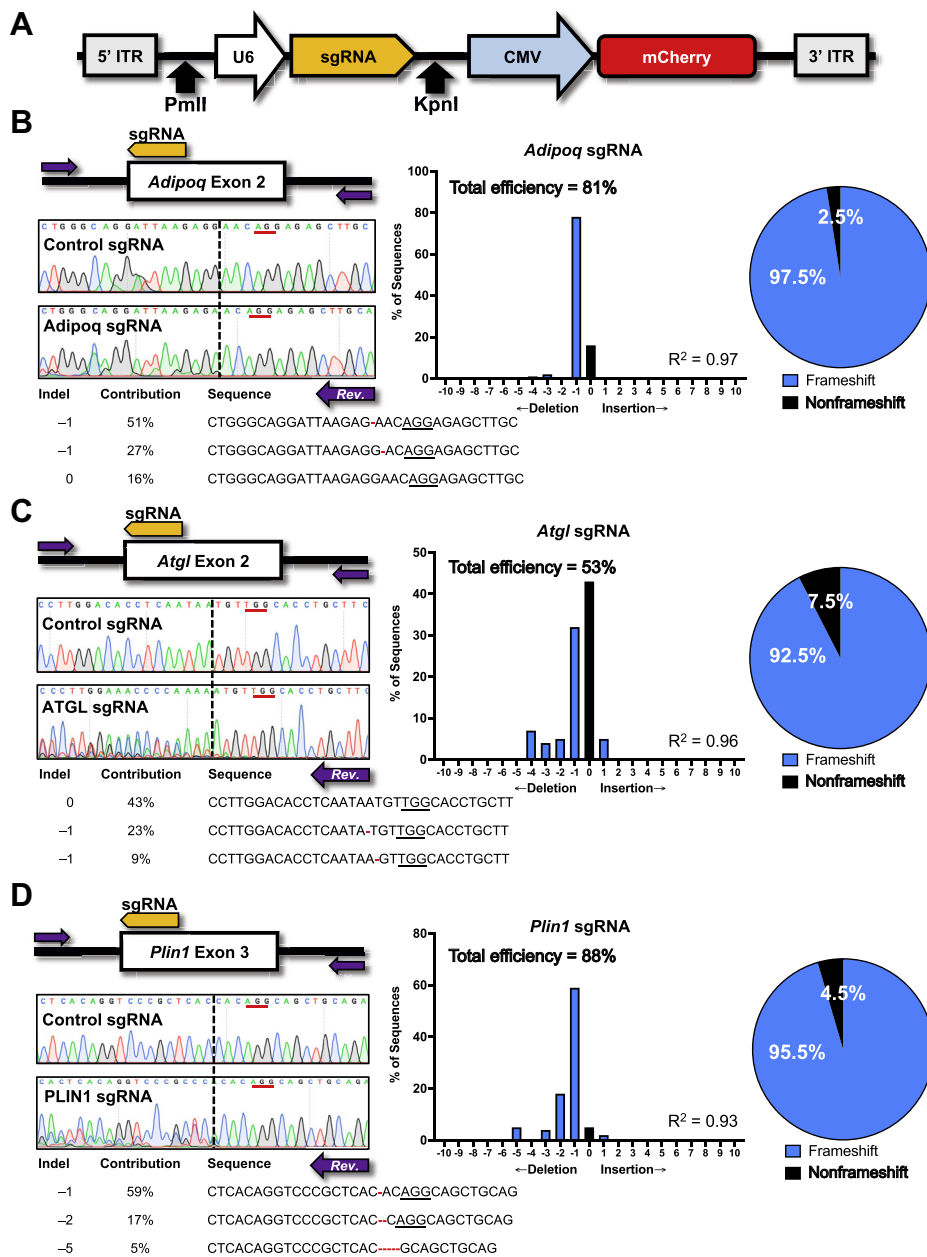


Figure 1. Transfection of adipocyte precursors with sgRNAs predominantly causes frameshift mutations in the target gene. A, U6 promoter-driven sgRNAs were cloned into an AAV expression vector using PmlI and KpnI. The expression vector also contained CMV promoter-driven mCherry and 5' and 3' ITRs to facilitate packaging of the cassette into AAV8. B–D, Sanger sequencing traces from Cas9-expressing adipocyte precursors transfected with AAV8-sgRNAs targeted to *Adipoq*, *Atgl*, and *Plin1*. For each target, the primers (purple arrows) were designed upstream and downstream of the sgRNA cut site (yellow arrow). Chromatograms of the reverse strand are shown, and the cut site (black dotted line) and PAM (red underline) are displayed for each sgRNA. The highest frequency indels for each sgRNA and percent contribution as determined by TIDE and the Synthego ICE Analysis tool are shown. Frameshift mutations were calculated by dividing the number of frameshifts over the total number of mutations, as estimated by the Synthego ICE Analysis tool. AAV, adeno-associated virus; Adipoq, adiponectin; ATGL, adipose triglyceride lipase; PAM, protospacer-adjacent motif; PLIN, perilipin; sgRNA, single guide RNA; TIDE, tracking of indels by decomposition.

To test sgRNAs targeting *Adipoq*, *Atgl*, and *Plin1*, AAV-expression vectors were transfected into primary adipocyte progenitor cells isolated from Rosa26-Cas9 knockin mice (24). The transfected cells were sorted for mCherry expression using flow cytometry, and DNA was analyzed by Sanger sequencing. Primers flanking sgRNA cut sites were used to sequence *Adipoq*, *Atgl*, and *Plin1*, and the traces were analyzed using the Tracking of Indels by Decomposition (TIDE) and the Synthego ICE Analysis tool (38). Corresponding sgRNA

efficiencies were observed in both the forward[†] and reverse sequence traces (Fig. 1, B–D). The Synthego ICE Analysis tool identified 1-base deletions as the predominant indel contribution across all sgRNAs tested. To calculate the total mutations resulting in a frameshift, we divided the number of frameshift mutations by the total number of predicted

[†] Data not shown.

BAd-CRISPR: Inducible gene knockout in BAT of adult mice

mutations. The frameshift mutations accounted for 97.5%, 92.5%, and 95.5% of the total mutations for sgRNAs targeting *Adipoq*, *Atgl*, and *Plin1*, respectively (Fig. 1, B–D). Analyzing CRISPR/Cas9-induced mutations using decomposition of Sanger sequence traces is an easy to use and cost-effective method for assessing a small number of samples (39). TIDE and next generation sequencing analyses have been shown to be highly correlated; however, frequencies calculated using TIDE often underrepresent true editing efficiency when compared with next generation sequencing (40). Thus, the true editing efficiency for each sgRNA is likely higher. After validating sgRNA efficiencies *in vitro*, AAV-expression vectors were used to generate AAVs encoding a sgRNA and mCherry fluorescent marker. For transducing adipose tissues, AAV serotype 8 (AAV8) has been used most extensively owing to its favorable tropism for brown and white adipocytes (27, 29, 32, 41–46).

BAd-CRISPR mice express Cas9 exclusively in BAT

Although AAV8 is the gold standard for transducing adipose tissues, its relatively small genome size (~4.7 kb) limits the ability to package *Streptococcus pyogenes* Cas9 with the sgRNA and mCherry transgene (27–29). Therefore, we developed a mouse line that expresses Cas9 specifically in brown adipocytes (BAd-CRISPR) by breeding two existing mouse lines: *Ucp1* promoter-Cre recombinase (B6.FVB-Tg (*Ucp1-cre*)1Evdr/J) and Cre-dependent Cas9-GFP (Rosa26-LSL-Cas9) (Fig. S2A) (10, 24). As expected, Cas9 is detected by immunoblot analyses in lysates from BAT of BAd-CRISPR mice but not from psWAT, parametrial WAT (pmWAT), or liver, nor is it found in tissues from mice lacking *Ucp1*-Cre expression (Fig. S2B). Confocal microscopy of freshly dissected tissues showed Cas9-GFP expression exclusively in BAT but not in psWAT, pmWAT, or liver (Fig. S2C). Thus, these mice are a suitable model to assess the effectiveness of CRISPR/Cas9 for inducible gene knockout specifically in brown adipocytes.

Local injection of AAV8-mCherry to interscapular BAT robustly transduces BAT with minimal leak to other tissues

Next, we optimized a delivery strategy using AAV8 to administer sgRNAs for BAd-CRISPR inducible gene knockout. Initially, we attempted tail vein injection or intraperitoneal injection of 100 μ l 10¹² vg/ml AAV8-mCherry to transduce all adipose tissues; however, both methods were unsuccessful and led to substantial transduction of liver. However, direct injection of AAV8 into adipose depots has been shown to significantly improve transduction efficiency and reduce vector accumulation in liver, heart, and lung (27, 29, 41). To test this approach, we directly injected 100 μ l 10¹² vg/ml AAV8-mCherry into interscapular BAT or psWAT and sacrificed mice after 14 days in accordance with previously established protocols (41, 47). In our hands, direct injection into psWAT transduced only a minority of white adipocytes; however, direct injection of interscapular BAT showed widespread and robust mCherry expression throughout the entire depot

(Fig. S3, A and B). After direct injection of BAT, a small number of cells in liver were also mCherry-positive, but mCherry was not detected in examined WAT depots (Fig. S3, A and B). Using quantitative PCR (qPCR), we found that *mCherry* mRNA expression was enriched in interscapular BAT after local injection, with low or undetectable expression in psWAT, pmWAT, liver, spleen, heart, lung, and kidney (Fig. S3B).

BAd-CRISPR induces efficient knockout of *Adipoq*, *Atgl*, *Fasn*, *Plin1*, or *Scd1* in brown adipocytes of adult mice

After validating robust BAT transduction using AAV8 direct injection, we next applied the BAd-CRISPR method to create inducible gene knockouts. We targeted genes that are highly expressed in brown adipocytes and administered 100 μ l 10¹² vg/ml AAV8-sgRNAs targeting *Adipoq*, *Atgl*, *Fasn*, *Plin1*, *Scd1*, or a control sgRNA, directly into the interscapular BAT of BAd-CRISPR mice (n = 3 or 4 mice). BAd-CRISPR mice were sacrificed 14 days postinjection, and BAT was homogenized to isolate mRNA and protein. Impressively, mRNA and protein expression for each target were reduced by 80 to 99% (Fig. 2, A–E). It should be noted that despite performing a transcardial perfusion, we detected albumin in BAT homogenate,[†] suggesting that blood was not completely cleared from the tissue. Thus, cellular ADIPOQ protein levels are likely reduced more than what is observed in the immunoblot (Fig. 2A). To further assess AAV8 transduction efficiency in BAT, we performed immunofluorescence for ATGL expression in BAd-CRISPR *Atgl* mice (Fig. 2F). ATGL was detected in only a few brown adipocytes (white arrows), indicating that the direct injection of AAV8 transduces the vast majority of brown adipocytes, and that expression of sgRNA and Cas9 efficiently ablates *Atgl*.

BAd-CRISPR *Atgl*, *Plin1*, and *Fasn* inducible knockouts recapitulate previously described BAT phenotypes

To investigate whether use of the BAd-CRISPR methodology recapitulates known knockout phenotypes in BAT, we further characterized BAd-CRISPR *Atgl*, BAd-CRISPR *Plin1*, and BAd-CRISPR *Fasn* inducible knockouts described in Figure 2 and compared our results with phenotypes reported using traditional transgenic approaches (48–52). BAd-CRISPR *Atgl* inducible knockout caused significant BAT hypertrophy compared with BAd-CRISPR control mice, and histological evaluation revealed a striking whitening of BAT (Fig. 3, A and B). These results mirror the phenotypes reported in global and BAT-specific inducible *Atgl* knockout mice, which also have marked hypertrophy and whitening of BAT (48, 49). By contrast, BAd-CRISPR *Plin1* inducible knockout led to a decrease in BAT weight coupled with the loss of multilocular brown adipocyte morphology, and the emergence of distinct unilocular lipid droplets dispersed throughout BAT (Fig. 3, A and B). These data are similar to the global *Plin1* knockout mouse models, which had smaller or complete loss of lipid droplets in BAT (50, 51). Interestingly, BAT weight was not altered in the two reported

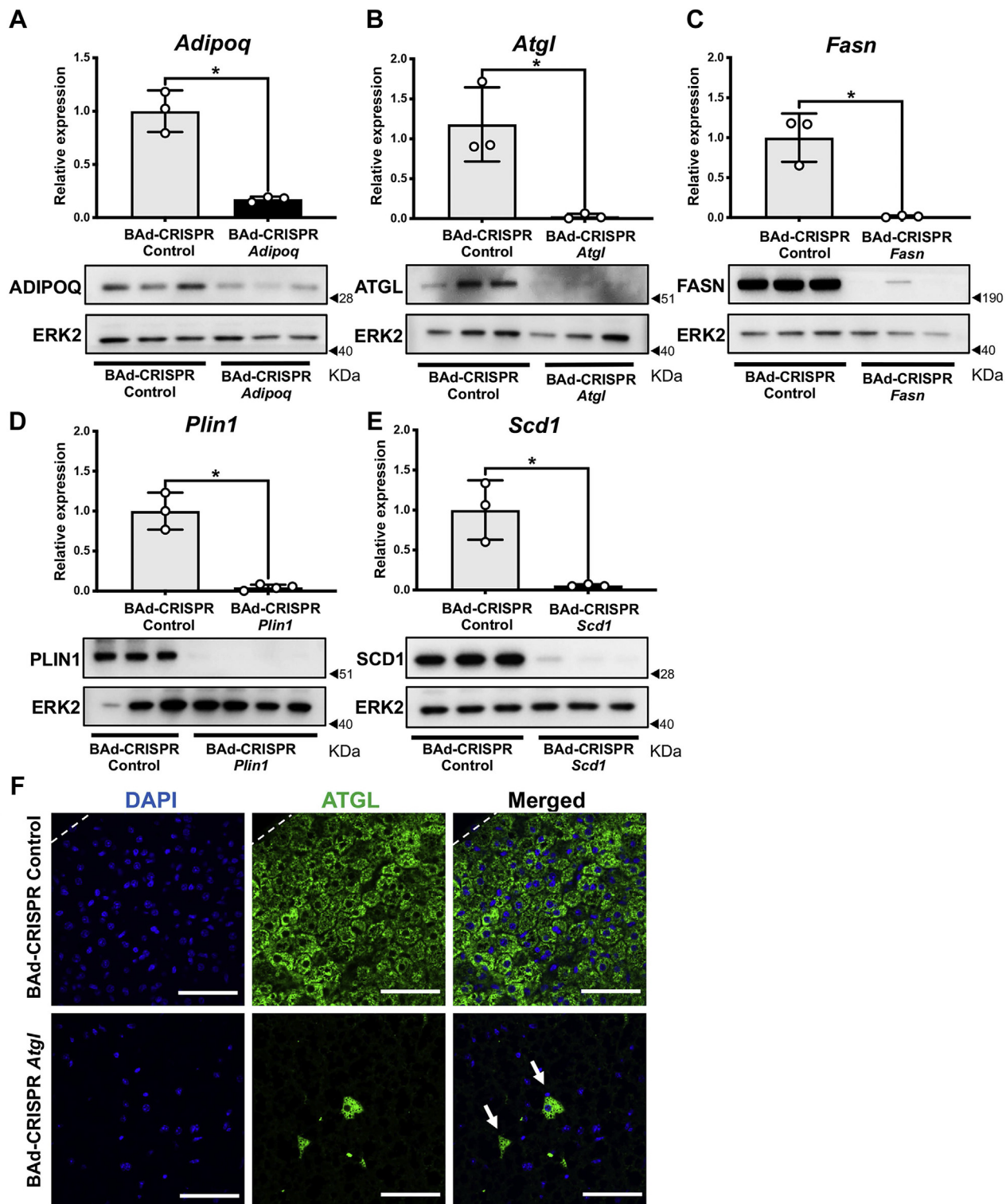


Figure 2. BAd-CRISPR induces efficient knockout of *Adipoq*, *Atgl*, *Fasn*, *Plin1*, or *Scd1* in brown adipocytes of adult mice. A–E, mRNA and protein expression in BAT of BAd-CRISPR mice administered 100 μ l 10^12 vg/ml AAV8-sgRNA targeting *Adipoq*, *Atgl*, *Fasn*, *Plin1*, *Scd1*, or control; mRNA expression was normalized to *Ppia* ($n = 3$ –4). F, immunofluorescence analysis of paraffin-sectioned BAT from BAd-CRISPR *Atgl* mice stained for DAPI and immunolabeled against ATGL; 600 \times magnification. The scale bar represents 50 μ m. White arrows indicate brown adipocytes that were not mutated. The data shown are from male (*Adipoq*, *Atgl*, *Fasn*, *Plin1*, and control) and female (*Scd1* and control) mice. The data are presented as mean \pm SD. * indicates significance at $p < 0.05$. AAV, adeno-associated virus; Adipoq, adiponectin; ATGL, adipose triglyceride lipase; BAd-CRISPR, brown adipocyte CRISPR; BAT, brown adipose tissue; CRISPR, clustered regularly interspaced short palindromic repeats; FASN, fatty acid synthase; PLIN, perilipin; SCD, stearoyl CoA desaturase; sgRNA, single guide RNA.

BAd-CRISPR: Inducible gene knockout in BAT of adult mice

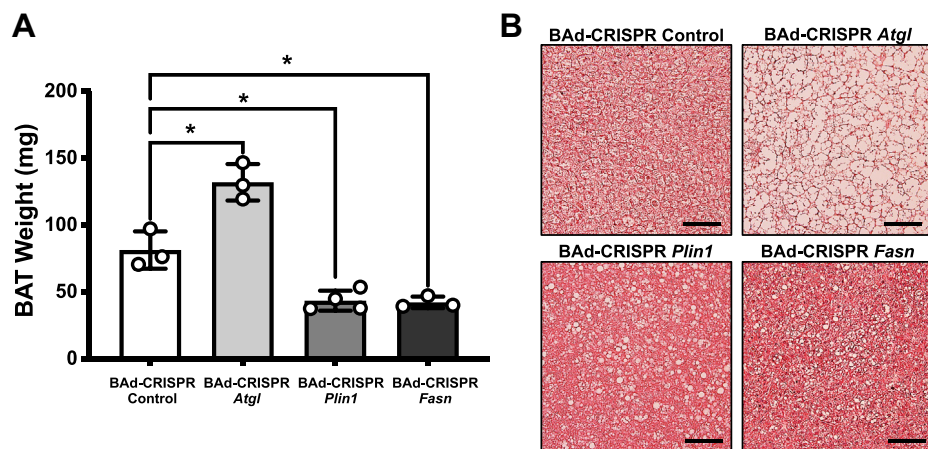


Figure 3. BAd-CRISPR Atgl, Plin1, and Fasn inducible knockouts recapitulate previously described BAT phenotypes. *A*, BAT weight (mg) of BAd-CRISPR mice administered 100 μ l 10^{12} vg/ml AAV8-sgRNAs for control, Atgl, Plin1, or Fasn ($n = 3-4$). *B*, H&E staining of BAT; 200 \times magnification. The scale bar represents 50 μ m. The data shown are from male mice and are presented as mean \pm SD. * indicates significance at $p < 0.05$. AAV, adenovirus; ATGL, adipose triglyceride lipase; BAd-CRISPR, brown adipocyte CRISPR; BAT, brown adipose tissue; CRISPR, clustered regularly interspaced short palindromic repeats; FASN, fatty acid synthase; PLIN, perilipin; sgRNA, single guide RNA.

Plin1 knockout models (50, 51). This difference may be explained by the fact that BAd-CRISPR inducible knockout mice lose PLIN1 expression in adulthood, whereas global knockout mice lack PLIN1 from birth. In addition, both reported *Plin1* knockout models are whole-body deletions, whereas BAd-CRISPR *Plin1* inducible knockout occurs specifically within brown adipocytes. Lastly, BAd-CRISPR *Fasn* mice showed a decrease in total lipid droplet size and BAT tissue weight relative to BAd-CRISPR control mice (Fig. 3, *A* and *B*). These data replicate the phenotype observed in *Ucp1*-Cre *FASN*^{fl/fl} mice, which had a reduction of lipid droplet size in brown adipocytes (52). Thus, BAd-CRISPR can be used to inducibly knockout genes of interest in brown adipocytes of adult mice, and its effects on several brown adipocyte genes phenocopy previously reported loss-of-function models.

BAd-CRISPR enables simultaneous knockout of two or three genes in brown adipocytes

To test whether BAd-CRISPR can be used to knockout multiple genes in BAT concurrently, we targeted *Atgl* and *Plin1* using two separate AAV8 vectors. We chose *Atgl* and *Plin1* as targets because they have opposing functions; ATGL hydrolyzes triacylglycerols, whereas PLIN1 protects against this hydrolysis (53, 54). Moreover, it has been established that *Atgl* knockout in BAT causes hypertrophy and whitening, whereas *Plin1* knockout in BAT decreases tissue size and causes a darker morphology; therefore we would have a visual phenotype with which to evaluate the feasibility of a double knockout (Fig. 3, *A* and *B*) (48–51). BAd-CRISPR mice and Rosa26-LSL-Cas9 mice lacking functional Cas9 (BAd-CRISPR Control) were administered 100 μ l 10^{10} vg/ml AAV8-sgRNA targeting *Atgl* alone, *Plin1* alone, or *Atgl* and *Plin1* in combination. BAd-CRISPR *Atgl* mice had profound whitening and BAT hypertrophy, whereas BAd-CRISPR *Plin1* mice had a darker BAT morphology and decreased tissue size (Fig. 4, *A* and *B*). By contrast, BAd-CRISPR *Atgl* + *Plin1* mice displayed

an intermediary morphology characterized by the presence of multilocular lipid droplets (Fig. 4, *A* and *B*).

Next, we explored whether three genes could be knocked out simultaneously. To accomplish this, BAd-CRISPR mice and Rosa26-LSL-Cas9 mice lacking functional Cas9 (BAd-CRISPR control) were administered 100 μ l 10^{12} vg/ml AAV8-sgRNA targeting *Atgl* alone, *Atgl* and *Plin1* together, or *Atgl*, *Plin1*, and *Ucp1* in combination (Fig. 4*C*). Immunoblot analyses showed loss of targeted protein expression specifically in BAT, whereas gene expression was unchanged in psWAT, eWAT, and liver,[†] indicating that CRISPR/Cas9 mutagenesis is BAT-specific (Fig. 4*C*). Of note, despite complete loss of UCP1 expression in BAT, we did not detect UCP1 expression or beigeing of psWAT when *Ucp1*-deficient mice were housed at 21 to 22 °C,[†] which is considered a mild cold stress (55, 56). Further, BAd-CRISPR is specific to interscapular BAT, with loss of ATGL and UCP1 in paravertebral BAT observed in only 1 to 2% of brown adipocytes.[†] Collectively, these data demonstrate that BAd-CRISPR is scalable for inducible knockout of multiple genes in interscapular BAT.

BAd-CRISPR ablates *Ucp1* expression in brown adipose tissue

The global *Ucp1* knockout mouse model has been extensively studied since it was first generated by Enerbäck *et al.* in 1997 (57). Thus, it is well known that UCP1-deficient mice (*Ucp1*^{−/−}) rely on compensatory mechanisms such as increased shivering, activation of futile cycles, or recruitment of beige/BRITE adipocytes to maintain body temperature when cold stressed (58). These adaptations allow *Ucp1*^{−/−} mice to tolerate a stepwise reduction in ambient temperature from thermoneutrality (~30 °C) to extreme cold (~10 °C); however, immediate cold exposure at 4 °C can prove lethal for mice lacking functional UCP1 (58–61). Although a plethora of papers have reported on molecular and physiologic consequences of constitutive global *Ucp1* knockout, whether similar effects are observed when *Ucp1* is inducibly knocked out of adult animals has not been explored.

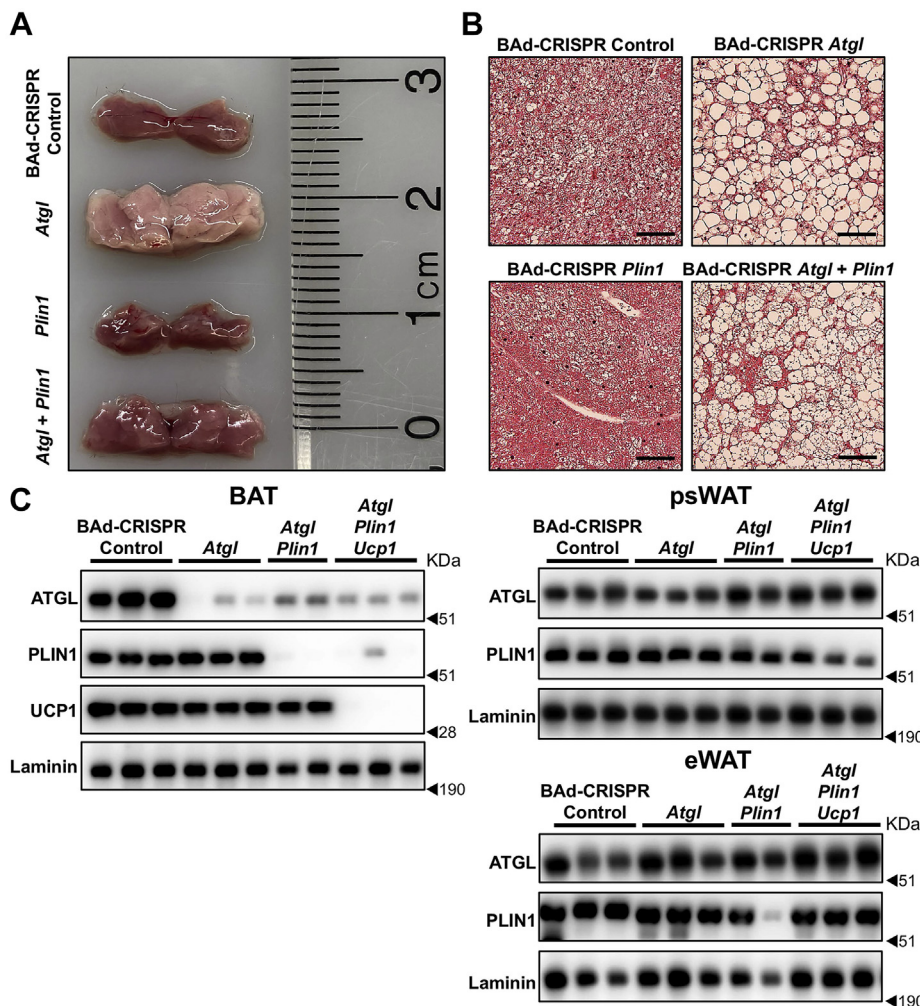


Figure 4. BAd-CRISPR enables simultaneous knockout of two or three genes in brown adipocytes. *A*, freshly dissected BAT from Rosa26-LSL-Cas9 + AAV8-*Atgl* sgRNA + AAV8-*Plin1* sgRNA (BAd-CRISPR Control), BAd-CRISPR *Atgl*, BAd-CRISPR *Plin1*, and BAd-CRISPR *Atgl* + *Plin1* mice administered 100 μ l 10¹⁰ vg/ml of the designated AAV8 ($n = 2$). *B*, H&E staining of BAT; 200 \times magnification. The scale bar represents 50 μ m. *C*, BAd-CRISPR mice were administered 100 μ l 10¹² vg/ml of a control AAV8-sgRNA or combinations of AAV8-sgRNAs to *Atgl*, *Plin1*, and *Ucp1* ($n = 2-3$). The expression of indicated proteins was determined by immunoblot analyses in the lysates from BAT, psWAT, and eWAT. Laminin is included as a loading control. The data shown are from male mice. AAV, adeno-associated virus; ATGL, adipose triglyceride lipase; BAd-CRISPR, brown adipocyte CRISPR; BAT, brown adipose tissue; CRISPR, clustered regularly interspaced short palindromic repeats; eWAT, epididymal white adipose tissue; FASN, fatty acid synthase; PLIN, perilipin; psWAT, posterior subcutaneous white adipose tissue; sgRNA, single guide RNA; UCP1, uncoupling protein 1.

To investigate BAd-CRISPR *Ucp1* mice further, we administered 100 μ l 10¹² vg/ml AAV8-*Ucp1* sgRNA directly into interscapular BAT and sacrificed mice at 0 (no virus), 2, 7, or 14 days post-injection to assess degree of knockout ($n = 3$ mice per timepoint). As expected, confocal microscopy of freshly dissected tissues at 14 days revealed robust mCherry expression in BAT, with no mCherry detected in psWAT or pmWAT, and a low signal detected in liver relative to BAT (Fig. 5A). Importantly, Cas9-GFP expression was exclusive to BAT and was not detected in other examined tissues (Fig. 5A). We also observed an increase in *mCherry* mRNA expression between 0 and 14 days (Fig. 5B). To assess for mutations in BAd-CRISPR *Ucp1* mice, we performed a genomic cleavage assay on cDNA as *Ucp1* mRNA is expressed specifically in brown adipocytes (Fig. 5C). We observed aberrant PCR product bands at 7 and 14 days postinjection but only the wildtype band at 0 and 2 days (Fig. 5C). We observed multiple

PCR products with or without addition of T7 endonuclease at 7 and 14 days, suggesting the amplification of mutations causing substantial deletions at the target site. To further confirm mutations, we performed Sanger sequencing on cDNA at the *Ucp1* sgRNA cut site and observed aberrant traces in mice at 14 days (Fig. 5D). Impressively, *Ucp1* mRNA expression was decreased by ~90% 2 days postinjection and by ~99% at 7 and 14 days (Fig. 5E). These results were further confirmed by immunoblot analyses, which showed dramatic reduction in UCP1 protein expression at 7 days and near total loss by 14 days without loss of ADIPOQ expression (Fig. 5F). Increased lipid accumulation, observed as whitening of BAT on histological evaluation, has been reported previously for *Ucp1*^{-/-} mice, and we also observe slight whitening in histological sections of BAT at 2, 7, and 14 days postinjection, relative to mice that were not administered AAV8-*Ucp1* sgRNA (day 0) (Fig. S4A) (57). UCP1 protein turnover occurs

BAd-CRISPR: Inducible gene knockout in BAT of adult mice

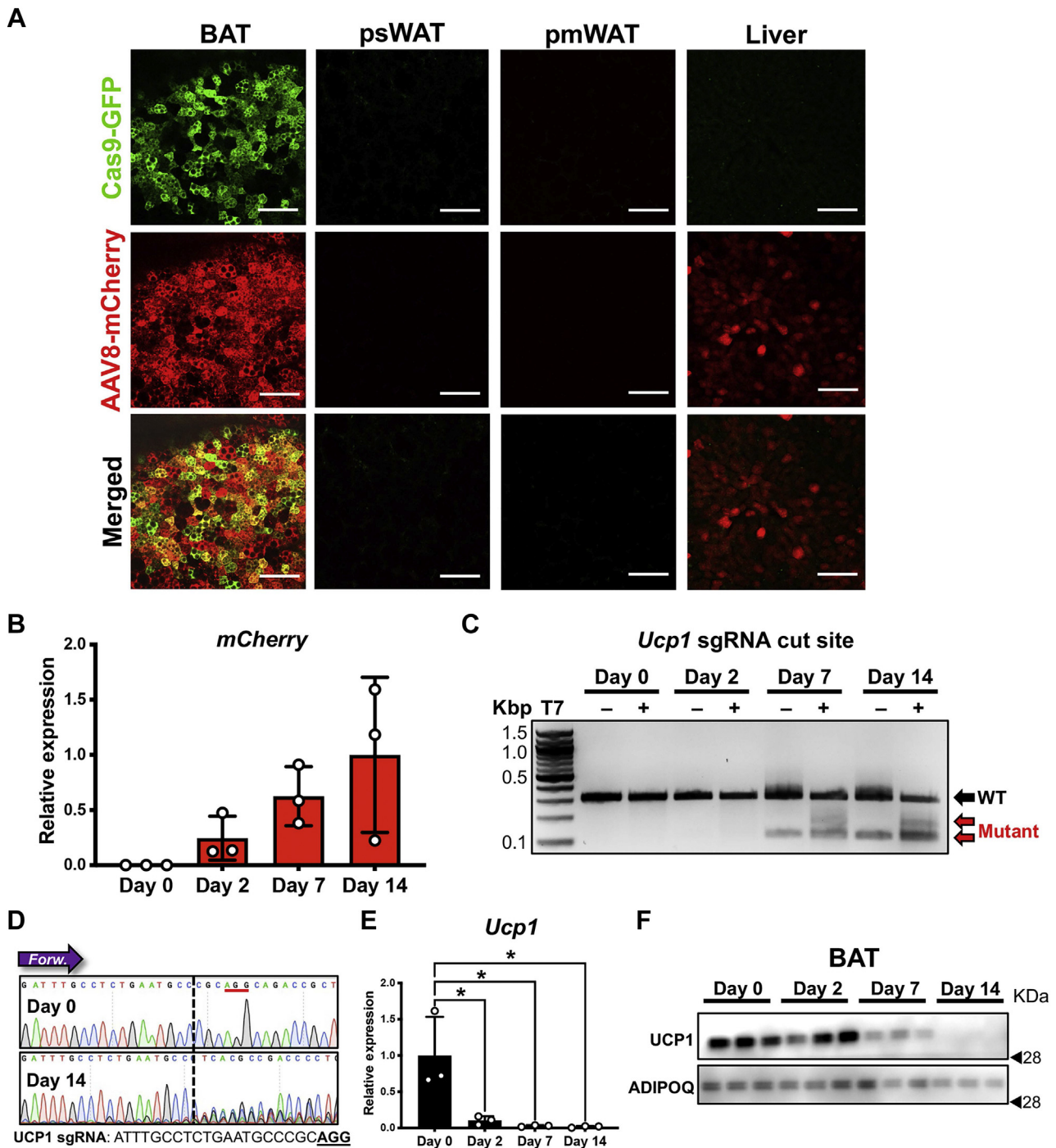


Figure 5. BAd-CRISPR ablates *Ucp1* expression in BAT. *A*, confocal micrographs of freshly dissected tissues from BAd-CRISPR *Ucp1* mice 14 days after 100 μ l 10^{12} vg/ml AAV8-*Ucp1* sgRNA injection; 200x magnification; the scale bar represents 50 μ m ($n = 3$). *B*, *mCherry* mRNA expression at each timepoint, RNA expression normalized to *Ppia* ($n = 3$ mice per timepoint). *C*, genomic cleavage assay of cDNA isolated from BAT. The red arrows indicate aberrant mutant PCR products. WT band = 320 bp. + or - indicates addition of the T7 endonuclease. *D*, Sanger sequencing traces of cDNA from 0 or 14 days postinjection. The expected cut site is indicated with a dashed line and the PAM is underlined in red. Below, the sgRNA sequence is shown, and the PAM is underlined and bolded. The purple arrow indicates the forward primer and sequencing direction. *E*, mRNA expression of *Ucp1* at each timepoint, RNA expression normalized to *Ppia* ($n = 3$ mice per timepoint). *F*, UCP1 and adiponectin protein expression at 0, 2, 7, or 14 days post AAV8-*Ucp1* sgRNA injection. The data shown are from female mice and are presented as mean \pm SD. * indicates significance at $p < 0.05$. AAV, adeno-associated virus; Adipoq, adiponectin; ATGL, adipose triglyceride lipase; BAd-CRISPR, brown adipocyte CRISPR; BAT, brown adipose tissue; CRISPR, clustered regularly interspaced short palindromic repeats; FASN, fatty acid synthase; PAM, protospacer-adjacent motif; PLIN, perilipin; pmWAT, parametrial white adipose tissue; psWAT, posterior subcutaneous white adipose tissue; sgRNA, single guide RNA; UCP1, uncoupling protein 1.

in the basal state by ~4 days and parallels the proteolytic rates of other mitochondrial proteins, consistent with our observation of protein loss starting at day 7 (62, 63).

To determine whether BAd-CRISPR *Ucp1* inducible knockout occurs as a result of CRISPR/Cas9 mutagenesis, we administered AAV8-*Ucp1* sgRNA to Rosa26-LSL-Cas9 mice that were bred to *Ucp1-Cre* mice (*Ucp1-Cre*⁺) or not (*Ucp1-Cre*⁻). UCP1 knockout occurred only when Rosa26-LSL-Cas9 mice were bred to the *Ucp1-Cre* background and therefore had functional Cas9 expression (Fig. S4, B and C). We also found that UCP1 knockout only occurred when BAd-CRISPR mice were administered AAV8-*Ucp1* sgRNA and not when administered AAV8-Control sgRNA (Fig. S4, D and E). To quantify transduction efficiency, we performed immunofluorescent analyses on fixed BAT from BAd-CRISPR *Ucp1* or BAd-CRISPR control mice. BAd-CRISPR *Ucp1* caused a near total loss of UCP1 expression in brown adipocytes, suggesting that viral transduction is almost 100% (Fig. S4F). We observed very few UCP1-positive cells dispersed throughout BAT (Fig. S4F). Although the anti-UCP1 antibody cross-reacted with endomucin-positive cells of the vasculature, loss of UCP1 in BAd-CRISPR *Ucp1* mice is readily observed (Fig. S4F). Collectively, these data provide strong evidence that CRISPR/Cas9 induces knockout of *Ucp1* in brown adipocytes of adult mice *in vivo*.

BAd-CRISPR *Ucp1* inducible knockout mice defend core body temperature and have elevated circulating FGF21

Next, we used BAd-CRISPR *Ucp1* mice to determine if adult mice maintain body temperature when cold stressed at 5 °C after inducible UCP1 knockout in BAT. Female 8- to 10-week-old mice were implanted with an intraperitoneal telemeter to monitor core body temperature 1 week before AAV8 administration. All mice were singly housed at room temperature (20–21 °C), and nest building materials were withheld throughout the study. We administered 100 μ l 10¹² vg/ml AAV8-*Ucp1* sgRNA or AAV8-Control sgRNA to the interscapular BAT (n = 4 or 5 mice) and the mice were allowed to recover for 14 days (Fig. 6A). The mice were then cold stressed at 5 °C for 24 h. BAd-CRISPR induced complete loss of UCP1 expression at both the mRNA and protein level (Fig. 6, B and C). Despite an apparent total knockout of UCP1 in interscapular BAT, there was no difference in body temperature when mice were housed at room temperature (20–21 °C) or cold stressed (5 °C) (Figs. 6, D and E and S5A). The same is true for the aforementioned *Ucp1*^{−/−} mice, which, when pre-acclimated to mild cold stress, are cold-tolerant (61). We did not observe changes to body weight, BAT weight, or average daily food intake between BAd-CRISPR control and BAd-CRISPR *Ucp1* mice (Fig. S5, B–D). Moreover, UCP1 protein expression was undetectable in inguinal WAT of these mice, suggesting that thermogenic mechanisms besides beige/BRITE adipogenesis are operative in BAd-CRISPR *Ucp1* mice (Fig. S5E). Interestingly, we did observe a significant increase in *Fgf21* expression in BAT (Fig. 6F). It has been reported that circulating FGF21 is increased in response to cold stress as a

compensatory mechanism for adaptive thermogenesis (34, 64, 65). Thus, we repeated this experiment using BAd-CRISPR *Ucp1* inducible knockout mice, *Ucp1*^{−/−} mice, and Rosa26-LSL-Cas9 (BAd-CRISPR Control) mice. Interestingly, we observed an “intermediate” increase in serum FGF21 concentrations in BAd-CRISPR *Ucp1* inducible knockout mice compared with *Ucp1*^{−/−} and BAd-CRISPR control mice after being cold stressed at 5 °C for 24 h (Fig. 6G). These data further support the role of FGF21 in adaptive thermogenesis (34, 64, 65).

Gene profiling of BAT from BAd-CRISPR *Ucp1* mice suggests peroxisomal lipid oxidation and increased protein synthesis/turnover as a compensatory thermogenic process

Although thermoneutrality in mice is approximately 30 °C, mice are typically housed at 20 to 22 °C and are therefore under a mild but chronic cold stress (55, 56). To explore potential mechanisms by which BAd-CRISPR *Ucp1* mice adapt to a moderate cold stress in the absence of UCP1, we performed RNA-Seq on BAT from mice administered 100 μ l 10¹² vg/ml AAV8-*Ucp1* sgRNA or AAV8-Control sgRNA. Of the >20,000 genes identified by RNA-Seq, 1056 were found to be differentially expressed. Consistent with the allele suppression observed using the BAd-CRISPR method, the most statistically significant difference was ~90% suppression of *Ucp1* mRNA in BAT of BAd-CRISPR *Ucp1* mice.[†] We then used gene set enrichment analysis (GSEA) to identify pathways that are significantly up- and down-regulated in response to inducible UCP1 knockout. GSEA indicated up-regulation of pathways involved in fatty acid metabolism, peroxisome function, unfolded protein response, protein secretion, and mTORC signaling (Fig. 7A). The pathways related to mitochondrial electron transport chain and heat production by uncoupling proteins were down-regulated, as was the citric acid cycle (Fig. 7A). Next, we mined GSEA pathways for genes that were significantly up- or down-regulated. We clustered genes based on pathways to generate a heatmap and found that BAd-CRISPR *Ucp1* inducible knockout mice have increased expression of peroxisome and lipid metabolism genes, which strongly suggests reliance on peroxisomal β-oxidation of fatty acids to generate heat (Fig. 7B) (66). Peroxisomal β-oxidation differs from mitochondrial β-oxidation in that peroxisomes lack a respiratory chain, and thus electrons from FADH₂ are transferred to O₂ to form H₂O₂, and energy is released as heat (66). Thus, it is likely that in response to acute loss of UCP1 expression in interscapular BAT, adult mice have increased reliance on peroxisomal β-oxidation to maintain thermoneutrality.

We also observed down-regulation of eight mitochondrial-encoded genes that encode proteins of the electron transport chain and coupled respiration, as well as the nuclear-encoded mitochondrial gene, *Ndufa4I2* (Fig. 7B). These data support work showing that UCP1-deficient BAT mitochondria exhibit dramatic reduction in proteins of the electron transport chain (67). However, we also observed induction of many nuclear-encoded mitochondrial genes, including substrate

BAd-CRISPR: Inducible gene knockout in BAT of adult mice

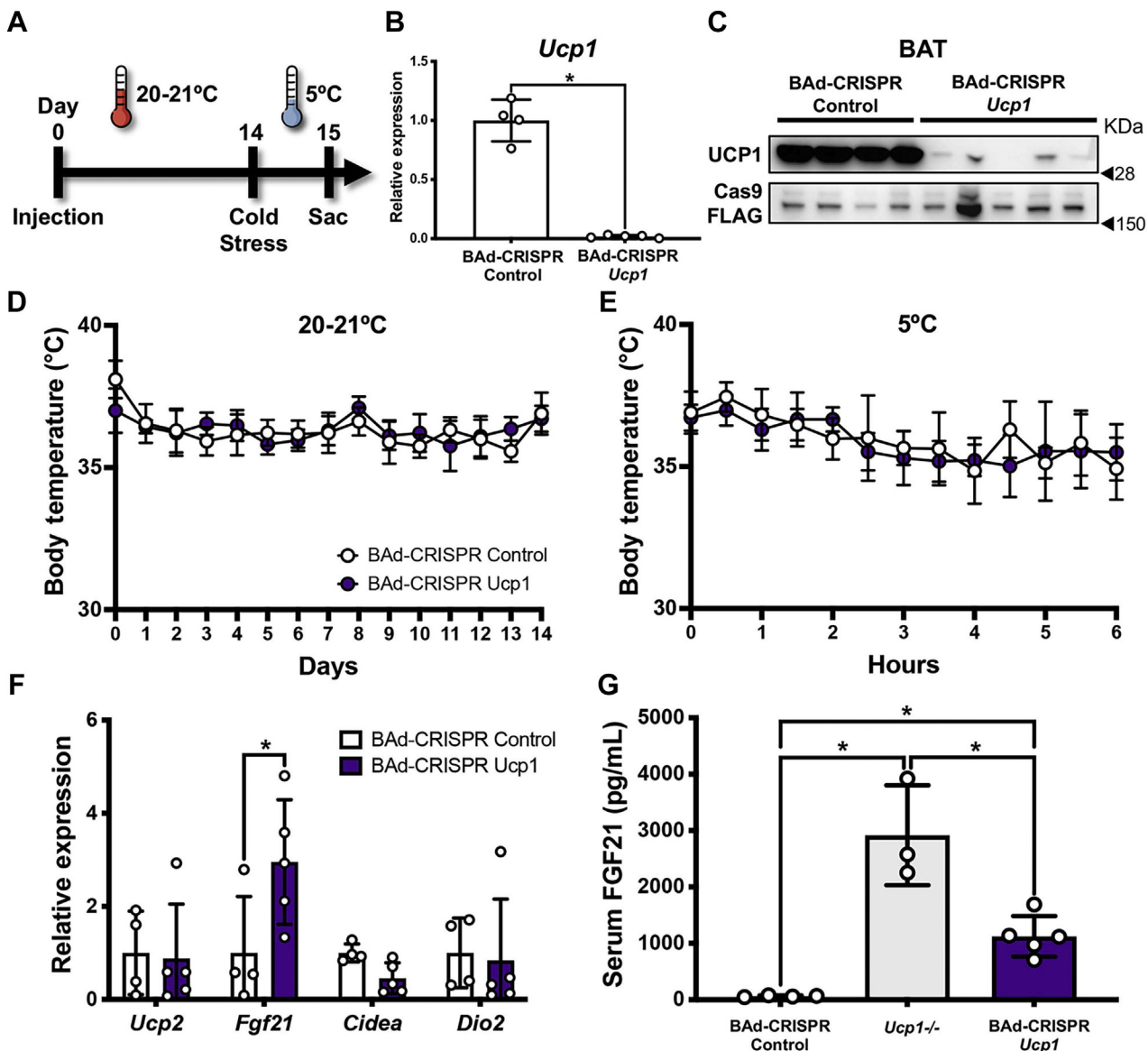


Figure 6. BAd-CRISPR *Ucp1* inducible knockout mice defend core body temperature and have elevated circulating FGF21. *A*, eight- to 10-week-old Rosa26-Cas9 knockin mice were implanted with a telemeter 7 days before injection with $100 \mu\text{l } 10^{12} \text{ vg/ml}$ AAV8-Control sgRNA or AAV8-*Ucp1* sgRNA and single-housed at 20 to 21 °C with no enrichment for 14 days after injection. The mice were cold stressed at 5 °C for 24 h and then sacrificed. *B*, *Ucp1* mRNA expression, mRNA normalized to *Ppia* ($n = 4$ or 5 mice). *C*, immunoblot showing UCP1 and Cas9 expression. *D* and *E*, body temperature at 20 to 21 °C and 5 °C. *F*, relative expression of thermogenic markers in BAT, mRNA normalized to *Ppia*. *G*, serum FGF21 concentrations in Rosa26-LSL-Cas9 (BAd-CRISPR Control), *Ucp1*^{-/-}, or BAd-CRISPR *Ucp1* mice ($n = 3$, 4, or 5 mice). The data shown are from female mice. The data are presented as mean \pm SD. * indicates significance at $p < 0.05$. AAV, adeno-associated virus; BAd-CRISPR, brown adipocyte CRISPR; BAT, brown adipose tissue; CRISPR, clustered regularly interspaced short palindromic repeats; FGF21, fibroblast growth factor 21; sgRNA, single guide RNA; UCP1, uncoupling protein 1.

transporters and subunits of ATP synthase (Fig. 7*B*). In addition, we observed elevated expression of eukaryotic initiation factors and tRNA synthetase genes, both of which are predicted to increase rates of protein translation (68, 69). We also detected up-regulation of genes encoding subunits of the proteasome, suggesting a futile cycle involving both increased synthesis and turnover of proteins (Fig. 7*B*). It may be that elevated *de novo* synthesis of proteins is required for adaptive thermogenesis and for protection against cellular stress in BAd-CRISPR *Ucp1* mice (70, 71). Lastly, we compared differentially expressed genes in BAd-CRISPR *Ucp1* mice and *Ucp1*^{-/-} mice housed at 20 °C (72). In total, 256 genes were found to overlap between datasets (Fig. 7*C*), including 45 of

the 130 heatmap genes shown in Figure 7*B*. Clustering of these 256 genes with Enrichr software identified pathways involved in the peroxisome, lipid metabolism, mitochondria, translation, and proteasome, providing further evidence for a common compensatory mechanism for adaptive thermogenesis in the absence of UCP1.

CRISPR/Cas9 does not lead to observable off-target mutations in the BAT of BAd-CRISPR *Ucp1* mice

CRISPR/Cas9 mutagenesis has been shown to have off-target effects at loci that bear similarity to the sgRNA sequence (73). These off-target mutations can impact genome

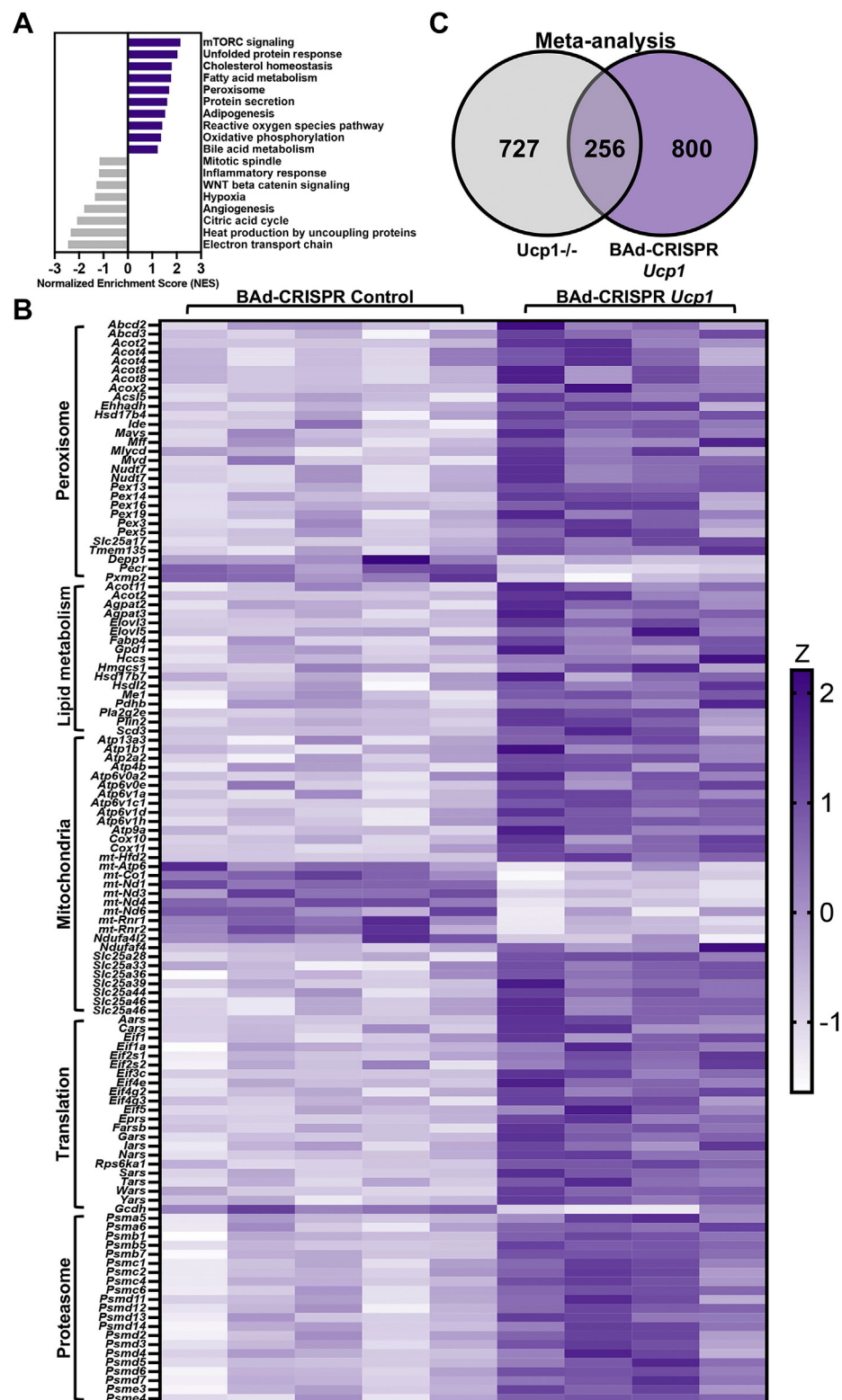


Figure 7. Gene profiling of BAT from BAd-CRISPR *Ucp1* mice suggests peroxisomal lipid oxidation and increased protein synthesis/turnover as a compensatory thermogenic process. *A*, gene set enrichment analysis (GSEA) of the most up- and down-regulated pathways. *B*, heatmap showing the expression of coordinately regulated genes associated with the peroxisome, lipid metabolism, mitochondria, protein translation, and the proteasome. *C*, Venn diagram depicting the overlap of significant differential gene expression of *Ucp1*^{-/-} and BAd-CRISPR *Ucp1* mice taken from GEO entry GSE127251. BAd-CRISPR, brown adipocyte CRISPR; BAT, brown adipose tissue; CRISPR, clustered regularly interspaced short palindromic repeats; UCP1, uncoupling protein 1.

BAd-CRISPR: Inducible gene knockout in BAT of adult mice

integrity and cause undesirable phenotypic changes. Using CRISPOR and the Synthego CRISPR Design tool, we identified seven off-target loci for the *Ucp1* sgRNA (Fig. 8A). The off-target loci had 3- or 4-base mismatches; no off-target sites contained fewer than 3-base mismatches. We focused on the highest predicted off-target site identified by both tools, which occurred in an intergenic space on chromosome 18, and off-target sites found within exons or introns of genes (Fig. 8A). To check for mutations at off-target sites, we performed unbiased whole genome sequencing on BAT from two BAd-CRISPR *Ucp1* mice. The whole genome sequencing data was analyzed using the Integrative Genome Viewer and CRISPRESSO2 (74, 75). We observed mutations in 36.1% of reads at the *Ucp1* locus compared with 1.78% at the intergenic space and 0.0% at all other sites, respectively (Fig. 8A). To probe the intergenic off-target site in more detail, we analyzed whole genome sequencing data from both BAd-CRISPR *Ucp1* mice using CRISPRESSO2 and found a single substitution at position one of the sgRNA sequence in one out of 51 total reads at this locus (Fig. 8B). CRISPRESSO2 did not identify insertions or deletions in reads at this off-target site. Next, we performed a genomic cleavage assay on genomic DNA from BAd-CRISPR

Ucp1 mice sacrificed at different timepoints and observed no aberrant mutant PCR or T7 cleavage products at the intergenic off-target site (Fig. 8C), suggesting that mutations at this off-target site are rare. In addition, we probed RNA-Seq data from BAd-CRISPR *Ucp1* mice and found no differences in expression of *Ypel2*, *Katnal1*, *Ago3*, *Adamts14*, or *Neu2*, all of which were potentially subject to off-target exonic or intronic mutations (Fig. 8D). Although one off-target site located within an intron of *Rftn1* had decreased mRNA expression in the BAd-CRISPR *Ucp1* mice, this locus has three mismatches proximal to the protospacer-adjacent motif, and we did not detect mutations with whole genome sequencing (Fig. 8, A and D). Thus, it is likely that reduction in *Rftn1* expression is secondary to UCP1-deficiency rather than the result of off-target mutagenesis. Taken together, these data suggest that BAd-CRISPR knockout does not lead to substantial off-target mutations.

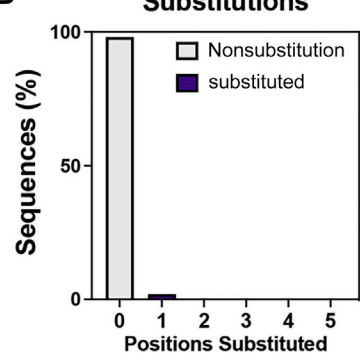
Discussion

Although viral CRISPR/Cas9 delivery has proven to be a powerful tool for manipulating the somatic genome in liver,

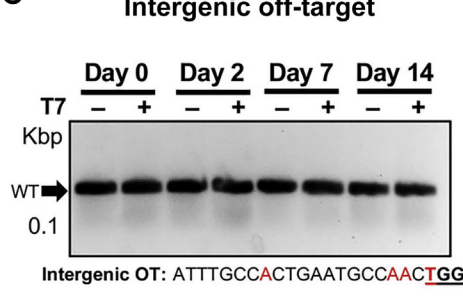
A

Gene	Sequence																								Mutations	±
<i>Ucp1</i>	A	T	T	T	G	C	C	T	C	T	G	A	A	T	G	C	C	C	G	C	36.1%	2.8				
Intergenic	A	T	T	T	G	C	C	A	C	T	G	A	A	T	G	C	C	A	A	C	1.8%	1.8				
<i>Ypel1</i>	A	T	T	T	G	C	C	T	C	T	G	A	A	T	G	T	C	T	C	C	0.0%	0				
<i>Katnal1</i>	C	T	T	T	G	C	C	T	C	T	G	A	G	T	G	C	C	A	G	C	0.0%	0				
<i>Ago3</i>	A	T	C	T	G	G	C	T	C	T	G	A	A	T	G	C	C	A	C	C	0.0%	0				
<i>Adamts14</i>	C	T	T	T	G	C	C	T	C	T	G	T	G	T	G	A	C	C	G	C	0.0%	0				
<i>Neu2</i>	T	T	T	T	G	C	C	A	C	T	G	A	A	T	G	C	C	A	G	A	0.0%	0				
<i>Rftn1</i>	A	T	T	T	G	C	C	T	C	T	A	A	A	G	G	A	C	C	C	C	0.0%	0				

B



C



D

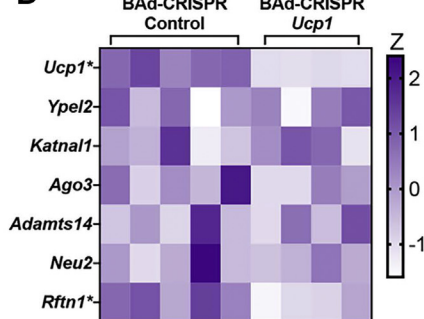


Figure 8. CRISPR/Cas9 does not lead to observable off-target mutations in BAT of BAd-CRISPR *Ucp1* mice. A, off-target sequence mismatches for *Ucp1* sgRNA predicted by CRISPOR and the Synthego sgRNA Design tool. The *Ucp1* sgRNA sequence is highlighted in yellow and base mismatches are colored red. Percent mutations were calculated using whole genome sequencing data visualized by the Integrative Genome Viewer (IGV) and CRISPRESSO2. B, indel characterization at the intergenic off-target determined by CRISPRESSO2. C, genomic cleavage assay at the intergenic off-target. WT band = 140 bp. D, heatmap of BAT gene expression for each off-target gene locus represented in the RNA-Seq dataset for BAd-CRISPR *Ucp1* mice. * indicates significance at $p < 0.05$. BAd-CRISPR, brown adipocyte CRISPR; BAT, brown adipose tissue; CRISPR, clustered regularly interspaced short palindromic repeats; sgRNA, single guide RNA; UCP1, uncoupling protein 1.

lung, heart, skeletal muscle, small intestine, thymus, and the central nervous system, its use has not been reported in BAT to date (19–26). The adipose field is heavily reliant upon the use of transgenic mice, which require significant time and financial investment. With nearly 40% of adults in the United States considered to be obese, more efficient strategies to study adipose tissues are required to improve our understanding of how these tissues contribute to metabolic disease and to identify potential therapies (76). BAd-CRISPR inducible gene knockout distills the laborious process of generating a transgenic mouse into two basic steps: constructing an AAV8-sgRNA and administering it to interscapular BAT of Cas9-expressing mice. Our method couples the novelty of CRISPR/Cas9 with the established Cre/LoxP system to enable highly efficient inducible gene knockout in BAT. Although we implemented this model for BAT using BAd-CRISPR mice, it is easily amendable to other cell types or tissues by crossing the Cre-dependent Rosa26-LSL-Cas9 with other tissue-specific promoter-driven Cre lines (24). Using our cloning strategy, a sgRNA can be incorporated into the AAV-expression vector, validated *in vitro*, used to generate any AAV serotype, and delivered to a tissue of interest. Our work has thus shown for the first time that CRISPR/Cas9 can be harnessed to significantly improve our understanding of BAT function. We anticipate that with further optimization, this methodology will become generally applicable to white, marrow, and other adipose depots.

We designed and validated highly efficient sgRNAs that caused frameshift mutations in cultured cells in >92% of the total sequences. In general, we prioritized sgRNAs that targeted early coding regions of genes to introduce frameshift mutations and disrupt translation of mRNA. We also observed profound suppression of mRNA expression for each targeted allele, suggesting a mechanism for inhibiting gene transcription. Rational design and validation of sgRNAs *in vitro* allowed us to select highly efficient sgRNAs for gene knockout *in vivo*. We showed that administration of a single AAV8-sgRNA to interscapular BAT resulted in near total knockout of *Adipoq*, *Atgl*, *Fasn*, *Plin1*, *Scd1*, or *Ucp1* specifically in brown adipocytes. We also demonstrated that multiple sgRNAs could be administered simultaneously using different AAV8 vectors to achieve concomitant knockout of up to three genes. Of note, we observed striking morphologic differences between BAT of mice administered AAV8-*Atgl* sgRNA, AAV8-*Plin1* sgRNA, or a combination of the two. Ideally, future iterations of BAd-CRISPR will entail multiple sgRNAs cloned into a single AAV expression vector. In our model, we were limited by packaging restrictions from the mCherry fluorescent marker, which we included to quantify transduction efficiency. However, based on our data, it is apparent that local AAV8 administration to the interscapular BAT leads to robust transduction and subsequent gene knockout. As such, the mCherry marker could be replaced with multiple U6 promoter-driven sgRNAs to different genomic targets. Packaging multiple sgRNAs into a single AAV is preferable to administering multiple AAVs to deliver single sgRNAs, as only one viral particle needs to transduce a brown adipocyte for

gene knockout. Moreover, packaging sgRNA along with Cas9 into one AAV could provide an all-in-one system for inducible gene knockout. Novel Cas9 orthologs smaller than *S. pyogenes* Cas9 (~1300 aa) such as *Neisseria meningitidis* Cas9 (1082 aa), *Staphylococcus aureus* Cas9 (1053 aa), *Campylobacter jejuni* Cas9 (984 aa), and *Geobacillus stearothermophilus* Cas9 (1089 aa) have all been identified for potential use to permanently modify the genome (77, 78). Thus, future iterations may include more compact, highly efficient Cas9 orthologs for an all-in-one AAV system.

BAd-CRISPR enabled us to generate the first inducible UCP1 knockout model and to determine that adult knockout mice can defend core body temperature when acutely cold stressed at 5 °C. Although UCP1 ablation was limited to interscapular BAT, mutations within brown adipocytes were sufficient to impact whole body physiology through the elevation of circulating FGF21, which is known to be up-regulated by *Ucp1* deficiency and in response to cold stress (34, 64, 65). RNA-Seq analysis identified dramatic changes to the transcriptome of BAT in BAd-CRISPR *Ucp1* mice. We observed an increase in genes associated with peroxisomal β-oxidation and lipid metabolism, suggesting that alternative adaptive thermogenic mechanisms are activated in response to inducible UCP1 loss in adult mice. We also found that inducible loss of UCP1 disrupted mitochondrial gene expression, with reduced mitochondrial-encoded electron transport chain genes, but induction of many nuclear-encoded mitochondrial genes. Gene profiling also suggests that thermogenesis in the absence of UCP1 may be accomplished by a futile cycle of increased protein synthesis and turnover. It is important to note that UCP1 loss was exclusive to the interscapular BAT, which is the largest BAT depot in rodents. However, the mice also have smaller BAT depots located in the periaortic, perirenal, paravertebral, and intercostal areas (79, 80). Therefore, it is likely that UCP1-mediated adaptive thermogenesis in these intact BAT depots helps to maintain body temperature in BAd-CRISPR *Ucp1* knockout mice.

Importantly, we did not detect evidence of substantial off-target mutations *in vivo* using unbiased whole genome sequencing and RNA-Seq analyses. It is known that the total number of mismatched base pairs is a determinant for *S. pyogenes* Cas9 efficiency, and that protospacer-adjacent motif-proximal mismatches are less tolerated than more distal mismatches (73). Hsu *et al.* (73) reported that three or more mismatches eliminated Cas9 cleavage activity at most genomic loci. In the example of *Ucp1* sgRNA, we did not observe significant mutations at seven off-target loci. Each of these loci contained 3 to 4 base mismatches. Although CRISPResso2 detected mutations in 1.8% of the reads at the intergenic off-target site on chromosome 18, we did not detect evidence of mutations at this locus using a genomic cleavage assay. Although we cannot definitively rule out off-target mutations at this site, the data suggests off-target mutations are quite rare, and thus are not likely to influence BAT physiology.

Although we have demonstrated that BAd-CRISPR is an efficient and versatile tool for generating inducible gene

BAd-CRISPR: Inducible gene knockout in BAT of adult mice

knockout in interscapular BAT, this method is not without its limitations. For instance, BAd-CRISPR permanently alters the genome of brown adipocytes only, and thus gene expression is not altered in stromal vascular cells even if transduced with AAV8-sgRNA. Thus, precursor cells that subsequently differentiate into brown adipocytes are unlikely to be mutated, and although adipocyte turnover in humans is estimated to be ~10% per year, long-term studies may necessitate additional injections for sustained knockout (81, 82). For broader application of BAd-CRISPR to brown adipocytes, stromal vascular cells, and precursor cells, the Rosa26-Cas9 knockin mouse can be used. In this model, all the cells express Cas9-GFP; therefore, gene knockout is enabled in all cell types within a tissue. Indeed, we have shown that local injection of AAV8 to the interscapular BAT also leads to detectable transduction in liver, where expression of sgRNAs would be expected to cause mutations in Rosa26-Cas9 knockin mice. However, incorporating microRNAs to the AAV vector can prevent transgene expression in off-target tissues. For example, Jimenez *et al.* (41) added liver and heart-specific microRNAs to AAV8, which significantly reduced transgene expression in each tissue, respectively. Thus, several strategies can be used to modify BAd-CRISPR for targeted gene knockout in whole tissues.

We have thus shown for the first time that CRISPR/Cas9 can be used for inducible gene knockout in BAT *in vivo*. Further optimization of AAV design and Cas9 isoforms can improve BAd-CRISPR to target white or marrow adipose tissues for gene knockout, inactivation, or overexpression. Importantly, we have shown that BAd-CRISPR enables the generation of transgenic animals with relative ease, less financial investment, and in significantly less time (*i.e.*, 1–2 months) compared with traditional approaches. Future work further characterizing the biological consequences of each inducible knockout in BAT of adult mice will be required. We hope that BAd-CRISPR will prove useful to the field of adipose tissue and beyond for CRISPR/Cas9 inducible gene knockout in somatic tissues.

Experimental procedures

sgRNA design and cloning

sgRNAs were designed using CRISPOR or the Synthego CRISPR Design tool (36). We selected sgRNAs that targeted early coding regions, did not have 0 or 1-base mismatch off-target sites, and had CFD scores >0.2. The 20-base sgRNA sequence was then used to synthesize a gBlocks Gene fragment that contained a U6 promoter and a gene-specific sgRNA scaffold, as well as the restriction sites PmlI and KpnI (Fig. S1) (IDT). The control sgRNA was designed to target *Gas*, but was repurposed as a control because it did not cause mutations or reduce *Gas* mRNA or protein. The AAV-expression vector plasmid was generously provided by the University of Michigan Vector Core. We inserted PmlI and KpnI restriction sites into the AAV-expression vector plasmid to enable cloning the U6-sgRNA gBlocks (NEB). The digested AAV expression vector plasmid and sgRNA gBlocks were separated using gel

electrophoresis and purified using the Wizard SV Gel and PCR Clean-Up System (Promega Corporation). sgRNA gBlocks were ligated into the AAV-expression vector using T4 DNA ligase according to the manufacturer's protocol (NEB). The AAV-sgRNA expression plasmid can be accessed from Addgene (Plasmid 174540).

AAV production

AAV-sgRNA expression plasmids were transformed into competent DH5α *E. coli* (Thermo Fisher Scientific). The plasmids were then isolated using the Qiagen Plasmid Maxi Kit (Qiagen). The plasmids were sequenced before being used to generate AAVs (Eurofins Genomics). All AAV8-sgRNAs were prepared by the University of Michigan Vector Core.

Cell culture

Primary adipocyte progenitor cells were isolated from the ears of Rosa26-Cas9 knockin mice (#024858, Jackson Lab), as previously described and cultured at 5% CO₂ (24, 83). Subconfluent cells were maintained in DMEM:F12 medium (Thermo Fisher Scientific) containing 10% fetal bovine serum (Sigma-Aldrich) and supplemented with 10 ng/ml recombinant basic fibroblast growth factor (PeproTech Inc). The AAV-sgRNA expression plasmids were transfected to Cas9 cells using Lipofectamine 3000 according to the manufacturer's protocol (Thermo Fisher Scientific). The cells were collected 4 days after transfection and sorted using the Sony MA900 Cell Sorter operated by the University of Michigan Flow Cytometry Core. The cells were lysed, and DNA was isolated using the Genomic Cleavage Detection Kit (Thermo Fisher Scientific).

Assessment of mutations

Mutations were assessed using TIDE (<https://tide.nki.nl/>), the Synthego ICE Analysis tool (www.ice.synthego.com), and the Genomic Cleavage Detection Kit (Thermo Fisher Scientific). For each of these assays, we designed primers that flanked the cut site and were >100 bp upstream and downstream from the sgRNA binding site. The DNA was amplified using Platinum SuperFi II DNA Polymerase (Thermo Fisher Scientific). For TIDE and the Synthego ICE Analysis, amplicons were sequenced (Eurofins Genomics), and traces were uploaded to the servers for analysis. The Genomic Cleavage Detection Kit was used according to the manufacturer's protocol. The sequencing primers are listed in Table S1.

Animals

All mouse strains for this study originated at Jackson Labs. Cre-dependent Cas9-GFP mice (Rosa26-LSL-Cas9, #026175) were bred with *Ucp1* promoter-Cre recombinase (B6.FVB-Tg(*Ucp1*-cre)1Evdr/J, #024670) to generate BAd-CRISPR mice. Rosa26-Cas9 knockin mice (#024858) were also used.

UCP1-deficient mice (*Ucp1*^{-/-}, #003124) were generously provided by Dr Liangyou Rui at the University of Michigan. The mice were housed in 12-h light/12-h dark cycles with free access to food and water. Room temperature was set at 20 to 21 °C with humidity at 28 to 38%. For cold stress studies, the mice were singly housed without nesting materials in thermal chambers for 24 h at 5 °C. The telemeters were implanted into the abdominal cavity to measure core body temperature, and surgeries were performed by the Michigan Mouse Phenotyping Center. All animal studies were approved by and conducted in compliance with the policies of the University of Michigan Institutional Animal Care and Usage Committee. Daily care of mice was overseen by the Unit for Laboratory Animal Medicine at the University of Michigan. Genotyping Primers are listed in [Table S1](#). All mice reported herein were BAd-Crispr except for the ATGL alone group in [Figure 4C](#), which expressed Cas9 globally.

AAV8 injection

AAV8 injections were performed, as previously described ([27](#), [47](#)). In brief, female or male 8- to 10-week-old BAd-CRISPR, Rosa26-LSL-Cas9, or Rosa26-Cas9 knockin mice were singly housed for 24 h before injections. The mice were anesthetized with 2 to 4% inhaled isoflurane in O₂, and a small area in the interscapular region was shaved to access BAT. A 1 to 2 cm incision was made, and the skin was peeled back to visualize the interscapular BAT. AAV8-sgRNAs were diluted in PBS (10¹² vg/ml or 10¹⁰ vg/ml as indicated) to a final volume of 100 µl and injected into the interscapular BAT by carefully inserting the needle into each lobe at 2 to 3 distinct spots and dispensing the virus (~50 µl per BAT lobe). Body weight and food intake were monitored daily to ensure mice remained healthy.

Quantitative PCR

Total RNA was purified from frozen tissue using RNA STAT-60 (Tel Test) according to the manufacturer's instructions. One µg of the total RNA was reverse-transcribed to cDNA using M-MLV Reverse Transcriptase (Invitrogen). qPCR was performed using a StepOnePlus System (Applied Biosystems). All the qPCR primers were validated with a cDNA titration curve, and product specificity was evaluated by melting curve analysis and gel electrophoresis of the qPCR products. Gene expression was calculated using a cDNA titration curve within each plate and then normalized to the expression of peptidylprolyl isomerase A (*Ppia*) mRNA. The qPCR primer sequences are listed in [Table S2](#).

RNAseq

Total RNA was isolated, as described using RNA STAT-60 (Tel Test) and treated with DNase. The samples were submitted to Beijing Genomics Institute (BGI) for quality control, library preparation, and paired-end sequencing to generate 101 base pair reads using DNB-SEQ-G400 platform. FASTQ files were downloaded for each sample. The quality

of raw read data was checked using FastQC (version 0.11.9) to identify features of the data that may indicate quality problems (low-quality scores, over-represented sequences, and inappropriate GC content) and filtered using fastp (version 0.21.0). The reads were aligned to the GRCm39 reference genome (Ensembl version 104) and quantified using STAR (version 2.7.7a). Quality control was performed on the read tables to ensure adequate depth, knockout of *Ucp1*, and to identify outlier samples. Differential expression analysis was carried out using DESeq2 (version 1.30.1). The plots were generated using variations or alternative representations of native DESeq2 plotting functions, ggplot2, plotly, and other packages within the R environment (version 4.0.3). To compare BAd-CRISPR *Ucp1* and *Ucp1*^{-/-} mice, RPKM values were taken from GEO entry GSE127251. The expression levels of genes between BAd-CRISPR *Ucp1* and *Ucp1*^{-/-} mice were compared using DESeq2. The resulting data were filtered for genes with significant differential expression (adjusted *p*-value < 0.05).

Immunoblot analysis

The frozen tissues were homogenized in 1% NP-40, 120 mM NaCl, 50 mM Tris-HCl; pH 7.4, 50 mM NaF, and 1× protease inhibitor cocktail (Sigma Aldrich), as previously described ([84](#), [85](#)). The homogenates were centrifuged at 18,000g for 10 min at 4 °C. Protein concentrations were determined using the BCA protein assay (Thermo Fisher Scientific). The samples were diluted to equal protein concentrations in lysis buffer and SDS sample buffer (20 mM Tris; pH 6.8, 2% SDS, 0.01% bromophenol blue, 10% glycerol, and 5% 2-mercaptoethanol) and heated at 95 °C for 5 min. The proteins were separated by SDS-PAGE on 4 to 12% gradient polyacrylamide gels (Invitrogen) and transferred to Immobilon PVDF membranes (Millipore). The membranes were blocked in 5% nonfat dried milk in Tris-buffered saline (pH 7.4) containing 0.05% Tween-20 (TTBS) for 30 min at room temperature and then immunoblotted with the indicated primary antibodies (1:1000) in 5% BSA in TTBS overnight at 4 °C. The blots were probed with horseradish peroxidase-conjugated secondary antibodies (1:5000) diluted in 5% nonfat dried milk in TTBS for 2.5 h at room temperature and visualized with Clarity Western ECL Substrate (Bio-Rad.). The antibodies are listed in [Table S3](#).

Histology

Soft tissues were harvested and fixed in 10% neutral buffered formalin overnight at 4 °C. The tissues were then dehydrated in an ethanol gradient (30% for 30 min, 50% for 30 min, and 70% indefinitely) and prepared for paraffin embedding. The paraffin-embedded tissues were sectioned at 5 µm thickness and stained with hematoxylin and eosin (H&E), as previously described ([86](#)). The stained sections were imaged using a Zeiss inverted microscope at 100× or 200× magnification.

BAd-CRISPR: Inducible gene knockout in BAT of adult mice

ELISA

Serum collected from mice was analyzed for circulating FGF21 using the Mouse/Rat FGF-21 Quantikine ELISA Kit (R&D Systems) by following the manufacturer's protocol.

Immunofluorescence analysis

Blocks of paraffin-embedded BAT from AAV8-*Atgl*, AAV8-*Plin1*, and AAV8-Control sgRNA injected mice ($n = 3$ mice) were sectioned at 5 μ m and floated onto microscope slides in a 39 °C water bath. Paraffin was removed from sections by three sequential 5-min washes in 100% xylene. The sections were next rehydrated in a series of ethanol washes from 100%, 95%, 70%, and 50% with each concentration consisting of two 10-min washes, followed by two 5-min washes in deionized water. Antigen retrieval was achieved by a 20-min incubation in sodium citrate buffer (10 mM sodium citrate and 0.05% Tween-20, pH 6.0) at 95 °C. The sections were cooled to room temperature, circled by a hydrophobic barrier, and then washed twice in deionized water for 5 min. The sections were permeabilized with 0.2% Triton X-100, 1× PBS for 10 min, and blocked in 10% normal donkey serum prepared in TNT buffer (0.1 M Tris-HCl pH 7.4 and 0.15 M NaCl, 0.05% Tween 20) for 1 h. Primary antibodies against ATGL (1:200), UCP-1 (1:100), endomucin (1:250), and PLIN1 (1:100) were prepared in 2.5% normal donkey serum in TNT buffer and then centrifuged at 15,000g for 10 min to remove aggregates. The sections were incubated in primary antibody dilutions for 16 h at 4 °C. The sections were washed three times in TNT buffer for 5, 10, then 15 min. The conjugated secondary antibodies against rabbit, goat, and rat were diluted 1:100 in TNT buffer and then centrifuged at 15,000g for 10 min to remove aggregates. The sections were incubated in secondary antibody dilutions for 1.5 h at room temperature and then washed twice for five then 10 min. Nuclei were stained with 14.3 μ M DAPI in PBS for 5 min and then washed twice in 1× PBS for 5 min. No. 1.5 coverslips were mounted to the slides with ProLong Gold mountant (Thermo Fisher Scientific) and cured for 2 days at room temperature before imaging. Immunofluorescent microscopy was performed using a Nikon A1 laser scanning confocal with Plan Apo VC 60× oil DIC N2 objective. The antibodies are listed in [Table S3](#).

Whole genome sequencing

Whole genome sequencing was performed by the University of Michigan Advanced Genomics Core using a NovaSeq 6000 system (Illumina, Inc). Genomic DNA quality control and NGS library prep services were all performed by the University of Michigan Advanced Genomics Core. FASTQ files were aligned using the mouse genome (Ensembl GRCm38) with bowtie2 (version 2.3.5.1). Indels were identified with CRISPRESSO2 (version 2.0.45) and visual inspection within the Integrative Genomics Viewer ([74](#)).

Statistics

All data are presented as mean \pm SD. When comparing two groups, significance was determined using Student's two-tailed

t test. When comparing multiple experimental groups, an ANOVA was followed by post hoc analysis with Dunnett's or Sidak's test as appropriate. The differences were considered significant at $p < 0.05$ and are indicated with asterisks.

Data availability

FASTQ files, along with count tables and metadata, can be accessed at GSE176453. All analysis code can be found at github.com/alanrupp/romanelli-jbiolchem-2021.

Supporting information—This article contains supporting information.

Acknowledgments—The authors would like to thank members of the MacDougald Laboratory for their insight and help preparing this article. We also thank several core facilities at the University of Michigan, including the Vector Core, Advanced Genomics Core, the Michigan Mouse Phenotyping Center (U2C DK110768), the Microscopy, Imaging, and Cellular Physiology Core (P30 DK020572), the Adipose Tissue Core of the MNORC (P30 DK089503), and the Flow Cytometry Core. Lastly, we thank Dr Kendall Clement of Massachusetts General Hospital for technical assistance with CRISPRESSO2, and Dr David Olson and the Molecular Genetics Core (P30 DK020572) for guidance and assistance throughout. This work was also funded by Research and Early Development, Cardiovascular, Renal and Metabolic Diseases, Bio-Pharmaceuticals R&D, AstraZeneca Ltd.

Author contributions—S. M. R., Z. L., H. M., B. S. L., and O. A. M. conceptualization; S. M. R., K. T. L., A. N., and A. C. R. data curation; S. M. R., K. T. L., A. N., and A. C. R. formal analysis; S. M. R., C. J. R., and O. A. M. funding acquisition; S. M. R., K. T. L., A. N., R. L. S., and B. S. L. investigation; S. M. R., K. T. L., A. N., A. C. R., and B. S. L. methodology; S. M. R. and O. A. M. writing—original draft; S. M. R., K. T. L., A. N., A. C. R., Z. L., H. M., R. L. S., C. J. R., and O. A. M. writing—review and editing; K. T. L. and A. N. visualization; O. A. M. resources; O. A. M., supervision; O. A. M. project administration.

Funding and additional information—This work was supported by grants from the NIH to O. A. M. (R01 DK121759 and R01 DK125513), S. M. R. (T32 GM835326 and F31 DK122723), K. T. L. (T32 DK071212 and F32 DK122654), R. L. S. (T32 DK101357 and F32 DK123887), and the American Diabetes Association to Z. L. (1-18-PDF-087). The content is solely the responsibility of the authors and does not necessarily represent the official views of the National Institutes of Health.

Conflict of interest—The authors declare that they have no conflicts of interest with the contents of this article.

Abbreviations—The abbreviations used are: AAV, adeno-associated virus; Adipoq, adiponectin; ATGL, adipose triglyceride lipase; BAd-CRISPR, brown adipocyte CRISPR; BAT, brown adipose tissue; CFD, cutting frequency determination; CRISPR, Clustered regularly interspaced short palindromic repeats; eWAT, epididymal white adipose tissue; FASN, fatty acid synthase; FGF21, fibroblast growth factor 21; GSEA, gene set enrichment analysis; PLIN1, perilipin 1; pmWAT, parametrial white adipose tissue; psWAT, posterior subcutaneous white adipose tissue; qPCR, quantitative PCR; SCD1, stearoyl coA desaturase 1; sgRNA, single guide RNA; TIDE,

Tracking of Indels by Decomposition; TTBS, tris buffered saline-tween; UCP1, uncoupling protein 1; WAT, white adipose tissue.

References

- Bagchi, D. P., Forss, I., Mandrup, S., and MacDougald, O. A. (2018) SnapShot: Niche determines adipocyte character I. *Cell Metab.* **27**, 264–264.e1
- Bagchi, D. P., and MacDougald, O. A. (2019) Identification and dissection of diverse mouse adipose depots. *J. Vis. Exp.* <https://doi.org/10.3791/59499>
- Wu, J., Bostrom, P., Sparks, L. M., Ye, L., Choi, J. H., Giang, A. H., Khandekar, M., Virtanen, K. A., Nuutila, P., Schaart, G., Huang, K., Tu, H., van Marken Lichtenbelt, W. D., Hoeks, J., Enerback, S., et al. (2012) Beige adipocytes are a distinct type of thermogenic fat cell in mouse and human. *Cell* **150**, 366–376
- Li, Z., and MacDougald, O. A. (2021) Preclinical models for investigating how bone marrow adipocytes influence bone and hematopoietic cellularity. *Best Pract. Res. Clin. Endocrinol. Metab.* **35**, 101547
- Alexander, C. M., Kasza, I., Yen, C. L., Reeder, S. B., Hernando, D., Gallo, R. L., Jahoda, C. A., Horsley, V., and MacDougald, O. A. (2015) Dermal white adipose tissue: A new component of the thermogenic response. *J. Lipid Res.* **56**, 2061–2069
- Trayhurn, P. (2005) Endocrine and signalling role of adipose tissue: New perspectives on fat. *Acta Physiol. Scand.* **184**, 285–293
- Rosen, E. D., and Spiegelman, B. M. (2006) Adipocytes as regulators of energy balance and glucose homeostasis. *Nature* **444**, 847–853
- Corsa, C. A. S., Walsh, C. M., Bagchi, D. P., Foss Freitas, M. C., Li, Z., Hardij, J., Granger, K., Mori, H., Schill, R. L., Lewis, K. T., Maung, J. N., Azaria, R. D., Rothberg, A. E., Oral, E. A., and MacDougald, O. A. (2021) Adipocyte-specific deletion of lamin A/C largely models human familial partial lipodystrophy type 2. *Diabetes* **70**, 1970–1984
- Lee, K. Y., Russell, S. J., Ussar, S., Boucher, J., Vernochet, C., Mori, M. A., Smyth, G., Rourk, M., Cederquist, C., Rosen, E. D., Kahn, B. B., and Kahn, C. R. (2013) Lessons on conditional gene targeting in mouse adipose tissue. *Diabetes* **62**, 864–874
- Kong, X., Banks, A., Liu, T., Kazak, L., Rao, R. R., Cohen, P., Wang, X., Yu, S., Lo, J. C., Tseng, Y. H., Cypress, A. M., Xue, R., Kleiner, S., Kang, S., Spiegelman, B. M., et al. (2014) IRF4 is a key thermogenic transcriptional partner of PGC-1alpha. *Cell* **158**, 69–83
- Krueger, K. C., Costa, M. J., Du, H., and Feldman, B. J. (2014) Characterization of Cre recombinase activity for *in vivo* targeting of adipocyte precursor cells. *Stem Cell Rep.* **3**, 1147–1158
- Rosenwald, M., Perdikari, A., Rulicke, T., and Wolfrum, C. (2013) Bi-directional interconversion of brite and white adipocytes. *Nat. Cell Biol.* **15**, 659–667
- Wang, Q. A., and Scherer, P. E. (2014) The AdipoChaser mouse: A model tracking adipogenesis *in vivo*. *Adipocyte* **3**, 146–150
- Jeffry, E., Berry, R., Church, C. D., Yu, S., Shook, B. A., Horsley, V., Rosen, E. D., and Rodeheffer, M. S. (2014) Characterization of Cre recombinase models for the study of adipose tissue. *Adipocyte* **3**, 206–211
- Bozec, A., Bakiri, L., Jimenez, M., Rosen, E. D., Catala-Lehnens, P., Schinke, T., Schett, G., Amling, M., and Wagner, E. F. (2013) Osteoblast-specific expression of Fra-2/AP-1 controls adiponectin and osteocalcin expression and affects metabolism. *J. Cell Sci.* **126**, 5432–5440
- Ye, R., Wang, Q. A., Tao, C., Vishvanath, L., Shao, M., McDonald, J. G., Gupta, R. K., and Scherer, P. E. (2015) Impact of tamoxifen on adipocyte lineage tracing: Inducer of adipogenesis and prolonged nuclear translocation of Cre recombinase. *Mol. Metab.* **4**, 771–778
- Jinek, M., Chylinski, K., Fonfara, I., Hauer, M., Doudna, J. A., and Charpentier, E. (2012) A programmable dual-RNA-guided DNA endonuclease in adaptive bacterial immunity. *Science* **337**, 816–821
- Doudna, J. A., and Charpentier, E. (2014) Genome editing. The new frontier of genome engineering with CRISPR-Cas9. *Science* **346**, 1258096
- Zafra, M. P., and Dow, L. E. (2016) Somatic genome editing goes viral. *Trends Mol. Med.* **22**, 831–833
- Dow, L. E. (2015) Modeling disease *in vivo* with CRISPR/Cas9. *Trends Mol. Med.* **21**, 609–621
- Sanchez-Rivera, F. J., Papagiannopoulos, T., Romero, R., Tammela, T., Bauer, M. R., Bhutkar, A., Joshi, N. S., Subbaraj, L., Bronson, R. T., Xue, W., and Jacks, T. (2014) Rapid modelling of cooperating genetic events in cancer through somatic genome editing. *Nature* **516**, 428–431
- Cheng, R., Peng, J., Yan, Y., Cao, P., Wang, J., Qiu, C., Tang, L., Liu, D., Tang, L., Jin, J., Huang, X., He, F., and Zhang, P. (2014) Efficient gene editing in adult mouse livers via adenoviral delivery of CRISPR/Cas9. *FEBS Lett.* **588**, 3954–3958
- Swiech, L., Heidenreich, M., Banerjee, A., Habib, N., Li, Y., Trombetta, J., Sur, M., and Zhang, F. (2015) *In vivo* interrogation of gene function in the mammalian brain using CRISPR-Cas9. *Nat. Biotechnol.* **33**, 102–106
- Platt, R. J., Chen, S., Zhou, Y., Yim, M. J., Swiech, L., Kempton, H. R., Dahlman, J. E., Parnas, O., Eisenhaure, T. M., Jovanovic, M., Graham, D. B., Jhunjhunwala, S., Heidenreich, M., Xavier, R. J., Langer, R., et al. (2014) CRISPR-Cas9 knockin mice for genome editing and cancer modeling. *Cell* **159**, 440–455
- Dow, L. E., Fisher, J., O'Rourke, K. P., Muley, A., Kastenhuber, E. R., Livshits, G., Tschaarganeh, D. F., Socci, N. D., and Lowe, S. W. (2015) Inducible *in vivo* genome editing with CRISPR-Cas9. *Nat. Biotechnol.* **33**, 390–394
- Guo, Y., VanDusen, N. J., Zhang, L., Gu, W., Sethi, I., Guatimosim, S., Ma, Q., Jardin, B. D., Ai, Y., Zhang, D., Chen, B., Guo, A., Yuan, G. C., Song, L. S., and Pu, W. T. (2017) Analysis of cardiac myocyte maturation using CASAAV, a platform for rapid dissection of cardiac myocyte gene function *in vivo*. *Circ. Res.* **120**, 1874–1888
- Gomez-Banoy, N., and Lo, J. C. (2017) Genetic manipulation with viral vectors to assess metabolism and adipose tissue function. *Methods Mol. Biol.* **1566**, 109–124
- Romanelli, S. M., and MacDougald, O. A. (2020) Viral and nonviral transfer of genetic materials to adipose tissues: Toward a gold standard approach. *Diabetes* **69**, 2581–2588
- Bates, R., Huang, W., and Cao, L. (2020) Adipose tissue: An emerging target for adeno-associated viral vectors. *Mol. Ther. Methods Clin. Dev.* **19**, 236–249
- Shen, Y., Cohen, J. L., Nicoloro, S. M., Kelly, M., Yenilmez, B., Henriquez, F., Tsagkaraki, E., Edwards, Y. J. K., Hu, X., Friedline, R. H., Kim, J. K., and Czech, M. P. (2018) CRISPR-delivery particles targeting nuclear receptor-interacting protein 1 (Nrrip1) in adipose cells to enhance energy expenditure. *J. Biol. Chem.* **293**, 17291–17305
- Kamble, P. G., Hetty, S., Vranic, M., Almby, K., Castillejo-Lopez, C., Abalo, X. M., Pereira, M. J., and Eriksson, J. W. (2020) Proof-of-concept for CRISPR/Cas9 gene editing in human preadipocytes: Deletion of FKBP5 and PPARG and effects on adipocyte differentiation and metabolism. *Sci. Rep.* **10**, 10565
- Yan, S., Kumari, M., Xiao, H., Jacobs, C., Kochumon, S., Jedrychowski, M., Chouchani, E., Ahmad, R., and Rosen, E. D. (2021) IRF3 reduces adipose thermogenesis via ISG15-mediated reprogramming of glycolysis. *J. Clin. Invest.* **131**, e144888
- Cannon, B., and Nedergaard, J. (2004) Brown adipose tissue: Function and physiological significance. *Physiol. Rev.* **84**, 277–359
- Villarroya, F., Cereijo, R., Villarroya, J., and Giralt, M. (2017) Brown adipose tissue as a secretory organ. *Nat. Rev. Endocrinol.* **13**, 26–35
- Cypress, A. M., Lehman, S., Williams, G., Tal, I., Rodman, D., Goldfine, A. B., Kuo, F. C., Palmer, E. L., Tseng, Y. H., Doria, A., Kolodny, G. M., and Kahn, C. R. (2009) Identification and importance of brown adipose tissue in adult humans. *N. Engl. J. Med.* **360**, 1509–1517
- Concordet, J. P., and Haeussler, M. (2018) CRISPOR: Intuitive guide selection for CRISPR/Cas9 genome editing experiments and screens. *Nucleic Acids Res.* **46**, W242–W245
- Doench, J. G., Fusi, N., Sullender, M., Hegde, M., Vainberg, E. W., Donovan, K. F., Smith, I., Tothova, Z., Wilen, C., Orchard, R., Virgin, H. W., Listgarten, J., and Root, D. E. (2016) Optimized sgRNA design to maximize activity and minimize off-target effects of CRISPR-Cas9. *Nat. Biotechnol.* **34**, 184–191
- Brinkman, E. K., Chen, T., Amendola, M., and van Steensel, B. (2014) Easy quantitative assessment of genome editing by sequence trace decomposition. *Nucleic Acids Res.* **42**, e168

BAd-CRISPR: Inducible gene knockout in BAT of adult mice

39. Shapiro, J., Iancu, O., Jacobi, A. M., McNeill, M. S., Turk, R., Rettig, G. R., Amit, I., Tovin-Recht, A., Yakhini, Z., Behlke, M. A., and Hendel, A. (2020) Increasing CRISPR efficiency and measuring its specificity in HSPCs using a clinically relevant system. *Mol. Ther. Methods Clin. Dev.* **17**, 1097–1107
40. Sentmanat, M. F., Peters, S. T., Florian, C. P., Connelly, J. P., and Pruitt-Miller, S. M. (2018) A survey of validation strategies for CRISPR-cas9 editing. *Sci. Rep.* **8**, 888
41. Jimenez, V., Munoz, S., Casana, E., Mallol, C., Elias, I., Jambrina, C., Ribera, A., Ferre, T., Franckhauser, S., and Bosch, F. (2013) *In vivo* adeno-associated viral vector-mediated genetic engineering of white and brown adipose tissue in adult mice. *Diabetes* **62**, 4012–4022
42. O'Neill, S. M., Hinkle, C., Chen, S. J., Sandhu, A., Hovhannissyan, R., Stephan, S., Lagor, W. R., Ahima, R. S., Johnston, J. C., and Reilly, M. P. (2014) Targeting adipose tissue via systemic gene therapy. *Gene Ther.* **21**, 653–661
43. Liu, X., Magee, D., Wang, C., McMurphy, T., Slater, A., During, M., and Cao, L. (2014) Adipose tissue insulin receptor knockdown via a new primate-derived hybrid recombinant AAV serotype. *Mol. Ther. Methods Clin. Dev.* **1**
44. Huang, W., McMurphy, T., Liu, X., Wang, C., and Cao, L. (2016) Genetic manipulation of brown fat via oral administration of an engineered recombinant adeno-associated viral serotype vector. *Mol. Ther.* **24**, 1062–1069
45. Huang, W., Liu, X., Queen, N. J., and Cao, L. (2017) Targeting visceral fat by intraperitoneal delivery of novel AAV serotype vector restricting off-target transduction in liver. *Mol. Ther. Methods Clin. Dev.* **6**, 68–78
46. Huang, W., Queen, N. J., and Cao, L. (2019) rAAV-mediated gene delivery to adipose tissue. *Methods Mol. Biol.* **1950**, 389–405
47. Balkow, A., Hoffmann, L. S., Klepac, K., Glode, A., Gnad, T., Zimmermann, K., and Pfeifer, A. (2016) Direct lentivirus injection for fast and efficient gene transfer into brown and beige adipose tissue. *J. Biol. Methods* **3**, e48
48. Haemmerle, G., Lass, A., Zimmermann, R., Gorkiewicz, G., Meyer, C., Rozman, J., Heldmaier, G., Maier, R., Theussl, C., Eder, S., Kratky, D., Wagner, E. F., Klingenspor, M., Hoefer, G., and Zechner, R. (2006) Defective lipolysis and altered energy metabolism in mice lacking adipose triglyceride lipase. *Science* **312**, 734–737
49. Schreiber, R., Diwoky, C., Schoiswohl, G., Feiler, U., Wongsiriroj, N., Abdellatif, M., Kolb, D., Hoeks, J., Kershaw, E. E., Sedej, S., Schrauwen, P., Haemmerle, G., and Zechner, R. (2017) Cold-induced thermogenesis depends on ATGL-mediated lipolysis in cardiac muscle, but not brown adipose tissue. *Cell Metab.* **26**, 753–763.e7
50. Tansey, J. T., Szalay, C., Gruia-Gray, J., Roush, D. L., Zee, J. V., Gavrilova, O., Reitman, M. L., Deng, C. X., Li, C., Kimmel, A. R., and Londos, C. (2001) Perilipin ablation results in a lean mouse with aberrant adipocyte lipolysis, enhanced leptin production, and resistance to diet-induced obesity. *Proc. Natl. Acad. Sci. U. S. A.* **98**, 6494–6499
51. Souza, S. C., Christoffolete, M. A., Ribeiro, M. O., Miyoshi, H., Strissel, K. J., Stancheva, Z. S., Rogers, N. H., D'Eon, T. M., Perfield, J. W., 2nd, Imachi, H., Obin, M. S., Bianco, A. C., and Greenberg, A. S. (2007) Perilipin regulates the thermogenic actions of norepinephrine in brown adipose tissue. *J. Lipid Res.* **48**, 1273–1279
52. Guilherme, A., Pedersen, D. J., Henchey, E., Henriques, F. S., Danai, L. V., Shen, Y., Yenilmez, B., Jung, D., Kim, J. K., Lodhi, I. J., Semenkovich, C. F., and Czech, M. P. (2017) Adipocyte lipid synthesis coupled to neuronal control of thermogenic programming. *Mol. Metab.* **6**, 781–796
53. Zechner, R., Zimmermann, R., Eichmann, T. O., Kohlwein, S. D., Haemmerle, G., Lass, A., and Madeo, F. (2012) FAT SIGNALS—lipases and lipolysis in lipid metabolism and signaling. *Cell Metab.* **15**, 279–291
54. Miyoshi, H., Perfield, J. W., 2nd, Souza, S. C., Shen, W. J., Zhang, H. H., Stancheva, Z. S., Kraemer, F. B., Obin, M. S., and Greenberg, A. S. (2007) Control of adipose triglyceride lipase action by serine 517 of perilipin A globally regulates protein kinase A-stimulated lipolysis in adipocytes. *J. Biol. Chem.* **282**, 996–1002
55. Lodhi, I. J., and Semenkovich, C. F. (2009) Why we should put clothes on mice. *Cell Metab.* **9**, 111–112
56. Seeley, R. J., and MacDougald, O. A. (2021) Mice as experimental models for human physiology: When several degrees in housing temperature matter. *Nat. Metab.* **3**, 443–445
57. Enerback, S., Jacobsson, A., Simpson, E. M., Guerra, C., Yamashita, H., Harper, M. E., and Kozak, L. P. (1997) Mice lacking mitochondrial uncoupling protein are cold-sensitive but not obese. *Nature* **387**, 90–94
58. Grimpel, K., Volker, M. N., Heppe, E. N., Braun, S., Heverhagen, J. T., and Heldmaier, G. (2014) Brown adipose tissue dynamics in wild-type and UCP1-knockout mice: In vivo insights with magnetic resonance. *J. Lipid Res.* **55**, 398–409
59. Meyer, C. W., Willershauser, M., Jastroch, M., Rourke, B. C., Fromme, T., Oelkrug, R., Heldmaier, G., and Klingenspor, M. (2010) Adaptive thermogenesis and thermal conductance in wild-type and UCP1-KO mice. *Am. J. Physiol. Regul. Integr. Comp. Physiol.* **299**, R1396–R1406
60. Golozoubova, V., Hohtola, E., Matthias, A., Jacobsson, A., Cannon, B., and Nedergaard, J. (2001) Only UCP1 can mediate adaptive nonshivering thermogenesis in the cold. *FASEB J.* **15**, 2048–2050
61. Meyer, C. W., Ootsuka, Y., and Romanovsky, A. A. (2017) Body temperature measurements for metabolic phenotyping in mice. *Front. Physiol.* **8**, 520
62. Moazed, B., and Desautels, M. (2002) Differentiation-dependent expression of cathepsin D and importance of lysosomal proteolysis in the degradation of UCP1 in brown adipocytes. *Can. J. Physiol. Pharmacol.* **80**, 515–525
63. Azzu, V., Jastroch, M., Divakaruni, A. S., and Brand, M. D. (2010) The regulation and turnover of mitochondrial uncoupling proteins. *Biochim. Biophys. Acta* **1797**, 785–791
64. Keipert, S., Kutschke, M., Lamp, D., Brachthauser, L., Neff, F., Meyer, C. W., Oelkrug, R., Kharitonov, A., and Jastroch, M. (2015) Genetic disruption of uncoupling protein 1 in mice renders brown adipose tissue a significant source of FGF21 secretion. *Mol. Metab.* **4**, 537–542
65. Keipert, S., Kutschke, M., Ost, M., Schwarzmayr, T., van Schothorst, E. M., Lamp, D., Brachthauser, L., Hamp, I., Mazibuko, S. E., Hartwig, S., Lehr, S., Graf, E., Plettenburg, O., Neff, F., Tschop, M. H., et al. (2017) Long-term cold adaptation does not require FGF21 or UCP1. *Cell Metab.* **26**, 437–446.e435
66. Lodhi, I. J., and Semenkovich, C. F. (2014) Peroxisomes: A nexus for lipid metabolism and cellular signaling. *Cell Metab.* **19**, 380–392
67. Kazak, L., Chouchani, E. T., Stavrovskaya, I. G., Lu, G. Z., Jedrychowski, M. P., Egan, D. F., Kumari, M., Kong, X., Erickson, B. K., Szpyt, J., Rosen, E. D., Murphy, M. P., Kristal, B. S., Gygi, S. P., and Spiegelman, B. M. (2017) UCP1 deficiency causes brown fat respiratory chain depletion and sensitizes mitochondria to calcium overload-induced dysfunction. *Proc. Natl. Acad. Sci. U. S. A.* **114**, 7981–7986
68. Torrent, M., Chalancon, G., de Groot, N. S., Wuster, A., and Madan Babu, M. (2018) Cells alter their tRNA abundance to selectively regulate protein synthesis during stress conditions. *Sci. Signal.* **11**, eaat6409
69. Pollo-Oliveira, L., and de Crecy-Lagard, V. (2019) Can protein expression be regulated by modulation of tRNA modification profiles? *Biochemistry* **58**, 355–362
70. Livneh, I., Cohen-Kaplan, V., Cohen-Rosenzweig, C., Avni, N., and Ciechanover, A. (2016) The life cycle of the 26S proteasome: From birth, through regulation and function, and onto its death. *Cell Res.* **26**, 869–885
71. Bartelt, A., Widenmaier, S. B., Schlein, C., Johann, K., Goncalves, R. L. S., Eguchi, K., Fischer, A. W., Parlakgul, G., Snyder, N. A., Nguyen, T. B., Bruns, O. T., Franke, D., Bawendi, M. G., Lynes, M. D., Leiria, L. O., et al. (2018) Brown adipose tissue thermogenic adaptation requires Nrf1-mediated proteasomal activity. *Nat. Med.* **24**, 292–303
72. Maurer, S. F., Fromme, T., Mocek, S., Zimmermann, A., and Klingenspor, M. (2020) Uncoupling protein 1 and the capacity for nonshivering thermogenesis are components of the glucose homeostatic system. *Am. J. Physiol. Endocrinol. Metab.* **318**, E198–E215
73. Hsu, P. D., Scott, D. A., Weinstein, J. A., Ran, F. A., Konermann, S., Agarwala, V., Li, Y., Fine, E. J., Wu, X., Shalem, O., Cradick, T. J., Marraffini, L. A., Bao, G., and Zhang, F. (2013) DNA targeting specificity of RNA-guided Cas9 nucleases. *Nat. Biotechnol.* **31**, 827–832

74. Pinello, L., Canver, M. C., Hoban, M. D., Orkin, S. H., Kohn, D. B., Bauer, D. E., and Yuan, G. C. (2016) Analyzing CRISPR genome-editing experiments with CRISPResso. *Nat. Biotechnol.* **34**, 695–697
75. Clement, K., Rees, H., Canver, M. C., Gehrke, J. M., Farouni, R., Hsu, J. Y., Cole, M. A., Liu, D. R., Joung, J. K., Bauer, D. E., and Pinello, L. (2019) CRISPResso2 provides accurate and rapid genome editing sequence analysis. *Nat. Biotechnol.* **37**, 224–226
76. Bluher, M. (2019) Obesity: Global epidemiology and pathogenesis. *Nat. Rev. Endocrinol.* **15**, 288–298
77. Wold, W. S., and Toth, K. (2013) Adenovirus vectors for gene therapy, vaccination and cancer gene therapy. *Curr. Gene Ther.* **13**, 421–433
78. Edraki, A., Mir, A., Ibraheim, R., Gainetdinov, I., Yoon, Y., Song, C. Q., Cao, Y., Gallant, J., Xue, W., Rivera-Perez, J. A., and Sontheimer, E. J. (2019) A compact, high-accuracy Cas9 with a dinucleotide PAM for in vivo genome editing. *Mol. Cell* **73**, 714–726.e4
79. Cinti, S. (2001) The adipose organ: Morphological perspectives of adipose tissues. *Proc. Nutr. Soc.* **60**, 319–328
80. Poher, A. L., Altirriba, J., Veyrat-Durebex, C., and Rohner-Jeanrenaud, F. (2015) Brown adipose tissue activity as a target for the treatment of obesity/insulin resistance. *Front. Physiol.* **6**, 4
81. Arner, P., Bernard, S., Salehpour, M., Possnert, G., Liebl, J., Steier, P., Buchholz, B. A., Eriksson, M., Arner, E., Hauner, H., Skurk, T., Ryden, M., Frayn, K. N., and Spalding, K. L. (2011) Dynamics of human adipose lipid turnover in health and metabolic disease. *Nature* **478**, 110–113
82. Sakaguchi, M., Fujisaka, S., Cai, W., Winnay, J. N., Konishi, M., O'Neill, B. T., Li, M., Garcia-Martin, R., Takahashi, H., Hu, J., Kulkarni, R. N., and Kahn, C. R. (2017) Adipocyte dynamics and reversible metabolic syndrome in mice with an inducible adipocyte-specific deletion of the insulin receptor. *Cell Metab.* **25**, 448–462
83. Mori, H., Prestwich, T. C., Reid, M. A., Longo, K. A., Gerin, I., Cawthorn, W. P., Susulic, V. S., Krishnan, V., Greenfield, A., and Macdougald, O. A. (2012) Secreted frizzled-related protein 5 suppresses adipocyte mitochondrial metabolism through WNT inhibition. *J. Clin. Invest.* **122**, 2405–2416
84. Mori, H., Dugan, C. E., Nishii, A., Benchamana, A., Li, Z., Cadenhead, T. S., Das, A. K., Evans, C. R., Overmyer, K. A., Romanelli, S. M., Peterson, S. K., Bagchi, D. P., Corsa, C. A., Hardij, J., Learman, B. S., et al. (2021) The molecular and metabolic program by which white adipocytes adapt to cool physiologic temperatures. *PLoS Biol.* **19**, e3000988
85. Bagchi, D. P., Nishii, A., Li, Z., DelProposto, J. B., Corsa, C. A., Mori, H., Hardij, J., Learman, B. S., Lumeng, C. N., and MacDougald, O. A. (2020) Wnt/beta-catenin signaling regulates adipose tissue lipogenesis and adipocyte-specific loss is rigorously defended by neighboring stromal-vascular cells. *Mol. Metab.* **42**, 101078
86. Parlee, S. D., Lentz, S. I., Mori, H., and MacDougald, O. A. (2014) Quantifying size and number of adipocytes in adipose tissue. *Methods Enzymol.* **537**, 93–122